AD

USAAVLABS TECHNICAL REPORT 69-63

EFFECT OF FIBER DIRECTION ON THE INSTABILITY OF SINGLE-LAYER RESIN-IMPREGNATED GLASS-CLOTH CYLINDERS UNDER TORSION

By

Milton Harold Bank, II

September 1971

EUSTIS DIRECTORATE
U. S. ARMY AIR MOBILITY RESEARCH AND DEVELOPMENT LABORATORY
FORT EUSTIS, VIRGINIA

CONTRACT DA 44-177-AMC-115(T)
STANFORD UNIVERSITY
STANFORD, CALIFORNIA

Unclassified
Security Classification

DOCUMENT CONTROL DATA - R & D

(Security classification of title, body of abstract and indexing annotation must be entered when the overall report is classified)

1. ORIGINATING ACTIVITY (Corporate author) Stanford University Stanford, Calif.	2a. REPORT SECURITY CLASSIFICATION Unclassified 2b. GROUP

3. REPORT TITLE
EFFECT OF FIBER DIRECTION ON THE INSTABILITY OF SINGLE-LAYER RESIN-IMPREGNATED GLASS-CLOTH CYLINDERS UNDER TORSION

4. DESCRIPTIVE NOTES (Type of report and inclusive dates)

5. AUTHOR(S) (First name, middle initial, last name)
Milton Harold Bank, II

6. REPORT DATE September 1971	7a. TOTAL NO. OF PAGES 61	7b. NO. OF REFS 18
8a. CONTRACT OR GRANT NO DA 44-177-AMC-115(T) b. PROJECT NO. Task 1F162204A17002 c. d.	9a. ORIGINATOR'S REPORT NUMBER(S) USAAVLABS Technical Report 69-63 9b. OTHER REPORT NO(S) (Any other numbers that may be assigned this report)	

10. DISTRIBUTION STATEMENT

Approved for public release; distribution unlimited.

11. SUPPLEMENTARY NOTES	12. SPONSORING MILITARY ACTIVITY Eustis Directorate, U.S. Army Air Mobility Research and Development Laboratory Fort Eustis, Virginia

13. ABSTRACT

128 tests on 65 single-layer open-weave glass-cloth resin-impregnated shells with five different fiber orientations were made. The report discussed these tests, the apparatus in which they were carried out, and the instrumentation used to make the appropriate observations. Additionally, it presents a statistical analysis of the results. This analysis indicates that fiber direction is significant. It influences both stability and stiffness. Generally speaking, the higher the strength the lower the stiffness.

It is significant to note that the Southwell Plot which is generally accepted for column data interpretation is shown equally pertinent to this problem.

DD FORM 1 NOV 68 1473

Unclassified
Security Classification

DISCLAIMERS

The findings in this report are not to be construed as an official Department of the Army position unless so designated by other authorized documents.

When Government drawings, specifications, or other data are used for any purpose other than in connection with a definitely related Government procurement operation, the United States Government thereby incurs no responsibility nor any obligation whatsoever; and the fact that the Government may have formulated, furnished, or in any way supplied the said drawings, specifications, or other data is not to be regarded by implication or otherwise as in any manner licensing the holder or any other person or corporation, or conveying any rights or permission, to manufacture, use, or sell any patented invention that may in any way be related thereto.

Trade names cited in this report do not constitute an official endorsement or approval of the use of such commercial hardware or software.

DISPOSITION INSTRUCTIONS

Destroy this report when no longer needed. Do not return it to the originator.

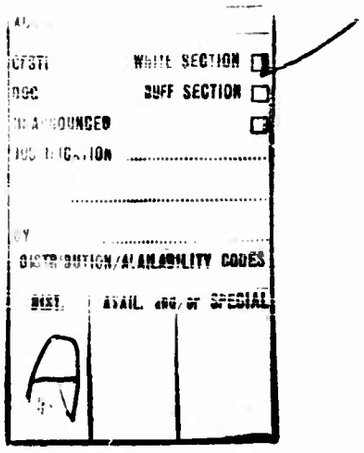

Unclassified

Security Classification

14. KEY WORDS	LINK A		LINK B		LINK C	
	ROLE	WT	ROLE	WT	ROLE	WT
Fiber Shells						
Torsion						
Buckling						
Instability						
Southwell Plot						

Unclassified

Security Classification

9359-71

DEPARTMENT OF THE ARMY
U. S. ARMY AIR MOBILITY RESEARCH & DEVELOPMENT LABORATORY
EUSTIS DIRECTORATE
FORT EUSTIS, VIRGINIA 23604

This program was carried out under Contract DA 44-177-AMC-115(T) with Stanford University.

The data contained in this report are the result of research conducted to study the effect of fiber orientation on the torsional strength and rigidity of fiberglass reinforced plastic shells. The primary fiber orientations studied were 0^{o}, 30^{o}, 45^{o}, 60^{o}, and 90^{o}.

The report has been reviewed by this Directorate and is considered to be technically sound. It is published for the exchange of information and the stimulation of future research.

The program was conducted under the technical management of Mr. James P. Waller, Structures Division.

Task 1F162204A17002
Contract DA 44-177-AMC-115(T)
USAAVLABS Technical Report 69-63
September 1971

EFFECT OF FIBER DIRECTION ON THE INSTABILITY OF SINGLE-LAYER RESIN-IMPREGNATED GLASS-CLOTH CYLINDERS UNDER TORSION

by

Milton Harold Bank, II

Prepared by

Stanford University
Department of Aeronautics and Astronautics
Stanford, California

for

EUSTIS DIRECTORATE
U.S. ARMY AIR MOBILITY RESEARCH AND DEVELOPMENT LABORATORY
FORT EUSTIS, VIRGINIA

SUMMARY

An experimental study of the torsional stability of single-layer open-weave glass-cloth plastic-impregnated shells is described. The design of a test apparatus and appropriate instrumentation is discussed. In all, 128 tests were made on 65 specimens for five different fiber orientations. Statistical analysis of the results showed that fiber directions affected both the torsional stiffness and buckling strength. Moreover, an increase in strength due to fiber orientation was always matched with a reduction in stiffness.

It is demonstrated, too, that the Southwell method of data analysis commonly used for struts is pertinent to the torsion problem. The agreement between the results of this interpretation of load-deflection data and the actual critical loads was, in general, good.

TABLE OF CONTENTS

FOREWORD

The research reported here is a part of a general investigation of composite structures being carried out by the Department of Aeronautics and Astronautics at Stanford University, sponsored by the U. S. Army Aviation Materiel Laboratories under Contract DA 44-177-AMC-115(T), Task 1F162204A17002.

LIST OF ILLUSTRATIONS

LIST OF ILLUSTRATIONS

LIST OF TABLES

INTRODUCTION

The behavior of shell bodies under various conditions of loading has been the subject of increasing research effort in recent years. Nash listed some 1,455 papers and books on the subject published prior to 1953[1], and 884 between 1954 and 1956[2]. It is reasonable to assume, in the light of space and weapons system applications, that this growth has continued.

Simultaneously, there has been a rapid development in materials consisting of fiber elements in resin matrices. The potential of these materials is universally recognized, but a lack of data on mechanical properties of the materials, a lack of adequate inspection techniques, and a lack of repeatable manufacturing processes for these materials have prevented full advantage being taken of their potential.[3]

The investigation presented here was undertaken as a part of a broad program of experimental and analytical study of fiber composite structures, touching on shell bodies and fiber resin materials. A previous investigation by Minecci[4] demonstrated that fiber direction does not materially influence the initial critical loads for instability in single-layer resin-impregnated glass-cloth shells subjected to uniform axial compression. The purpose of this research was to study the effect of fiber direction on torsional strength and rigidity of such shells.

DISCUSSION OF THE PROBLEM

Very few theoretical or experimental studies have been made for heterogenous aeolotropic bodies, and the ones that are available are primarily concerned with plywood structures. Cheng and Ho[5] have published a small-deflection treatment of the stability of heterogeneous, aeolotropic, cylindrical shells under combined loading, and Ho and Cheng[6] have compared this work with limited test data. This work, however, is based on the classical Kirchoff-Love non-deformable normals hypothesis, a hypothesis which Ambartsumian[7] believes will have to be abandoned before a complete theory of perfect shells made of substantially anisotropic materials can be developed.

The need for experimental knowledge which can form a basis for analytical study of heterogeneous aeolotropic shells is clear. Thus, it was decided that the investigation of single-layer resin-impregnated glass-cloth shells should be extended to study the question of how fiber direction influences the critical torsional load for such a body.

OUTLINE OF THE RESEARCH PROGRAM

As explained previously, the essential purpose of the research was to provide an experimental background on fiber cylinders which could aid in the analytical study of such bodies. Because of the variances which naturally occur in shells of this type, it was decided that a large number of test vehicles would be required. Thus, the investigation was of necessity restricted to one exterior geometry since, by so doing, the time devoted to fabrication of specimens could be drastically reduced and the amount of testing would consequently be maximized. The internal fiber angle of the specimens was varied.

It is obvious that if a sufficiently large number of observations are available, valid conclusions can be drawn from a statistical analysis of the data. Such conclusions, however, must of necessity bear primarily on the probable behavior of imperfect bodies under realized test conditions. Thus, the program included a series of tests which were made on a restricted number of specimens to study whether or not the radial displacement of the shell wall under torsional loading could be directly associated with load level, as is implied by the general theory of elastic stability presented by Westergaard[8].

DESCRIPTION OF THE SPECIMENS

The shells used in this program had nominally identical exterior geometry. They were cylindrical, 10.75 $\pm$0.03 inches long, and 4.7555 $^{+0.010}_{-0.000}$ inches in diameter.

They were fabricated from an open-weave glass cloth. This cloth, E-Volan A glass fiber, had 18 fibers per inch in the warp and 16 fibers per inch in the fill. The manufacturer's designation was Type 2P 127 "Boatcloth". The cloth was stabilized by an epoxy resin system made up of 100 parts of Epon 825 to 11 parts of diethylene-triamine hardener.

MANUFACTURE OF THE SPECIMENS

An appropriate length of glass cloth was cut from the bolt, examined for imperfections, and smoothed, and the fibers were straightened and aligned. The cloth was transferred to a warm teflon-covered aluminum plate over which resin had been evenly spread using a paint roller. The roller was used again on the glass cloth and resin to impregnate the fibers with resin as evenly as possible.

The cloth was partially cured at 150° for 15 minutes (Figure 1), producing a flexible, easily handled material from which blanks of proper size with the desired fiber orientation were cut. These rectangular elements were final-cured in a cylindrical curing oven (Figure 2) in which they were simultaneously spun and heated. The rotation forced the material into a cylindrical shape, and the heating completed the curing process.

The heat source for the curing oven was a pair of quartz tubular heaters mounted on a central axial shaft in the oven. The rated output of the heaters is 1,000 watts at 230 volts; however, they were used at 120 volts. During the 30-minute hot-forming and curing cycle, they raised the temperature of the blanks to a maximum of 250°.

The specimens were lap-seamed on a warm mandrel (Figure 3), using Duco cement as the bonding agent. The resultant seam was slightly stronger than the rest of the specimen; it was composed of two layers of glass cloth rather than one. However, the buckle patterns went through the seam in every test with no distortion other than a slight reduction in size (Figure 11a and 11e) This was taken as evidence that the seam was not, in fact, materially stronger than the rest of the shell body.

Seaming on the mandrel resulted in close control of the diameter of the specimens. Control of the length was accomplished by trimming off the ends of the seamed shells using a high-speed cutting tool mounted on a lathe tool post holder (Figure 4) while the shell was rotated at 460 rpm. In this fashion, the ends were cut square and the length was held within 1/32 inch of the desired 10.75 inches.

The specimens were weighed three times during the manufacturing process. First, the cured cylindrical blank was weighed to establish a base; second, the seamed blank was weighed, permitting determination of the weight of glue in the seam; and third, the finished specimen was weighed. Specimen weight was taken as final weight less glue weight; weight of the glue cut off during the trimming operation was less than 0.1 gram and was neglected.

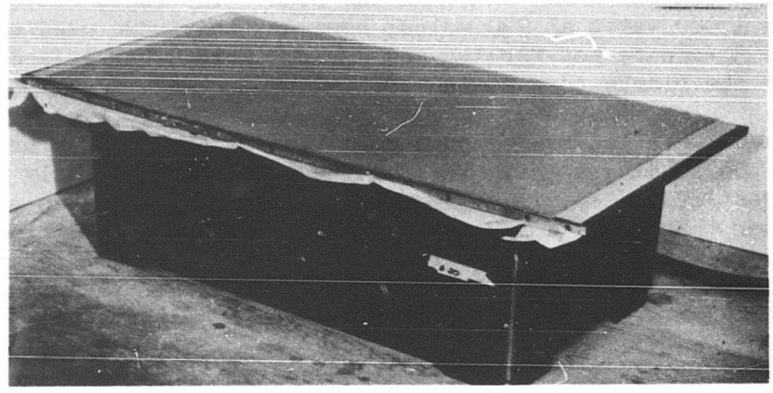

Figure 1. Initial Curing of Material for Specimens.

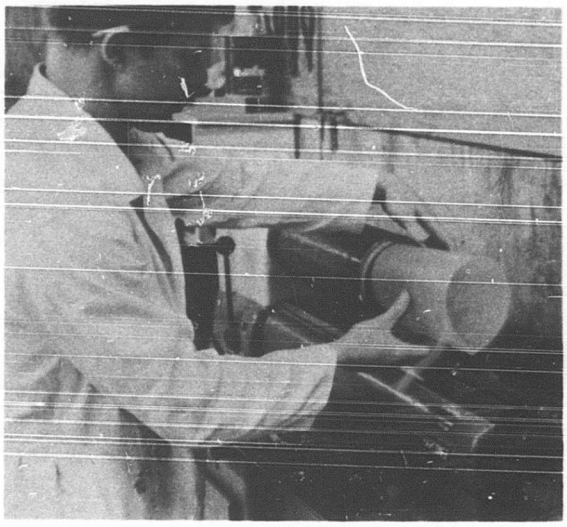

a. Inserting Specimen Blanks in Curing Oven.

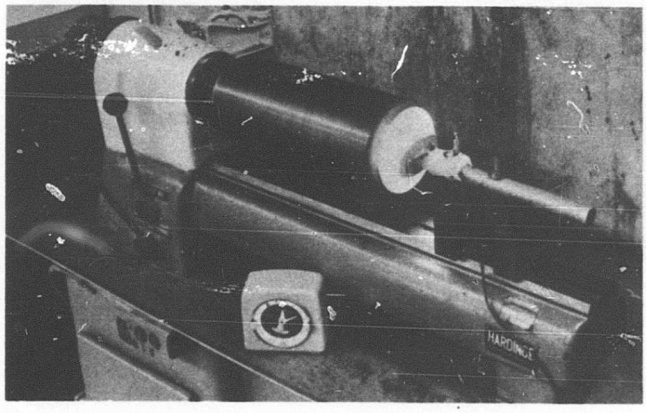

b. Final-Curing Oven in Operation.

Figure 2. Curing Oven.

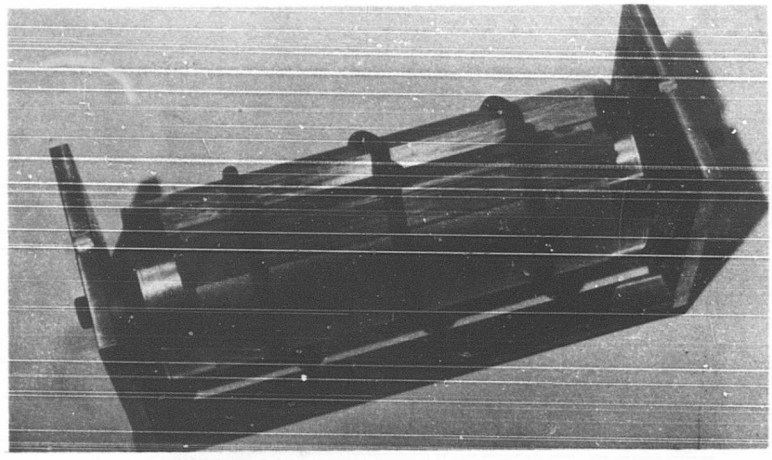

Figure 3. Specimen Blank Ready for Seaming on Warm Mandrel.

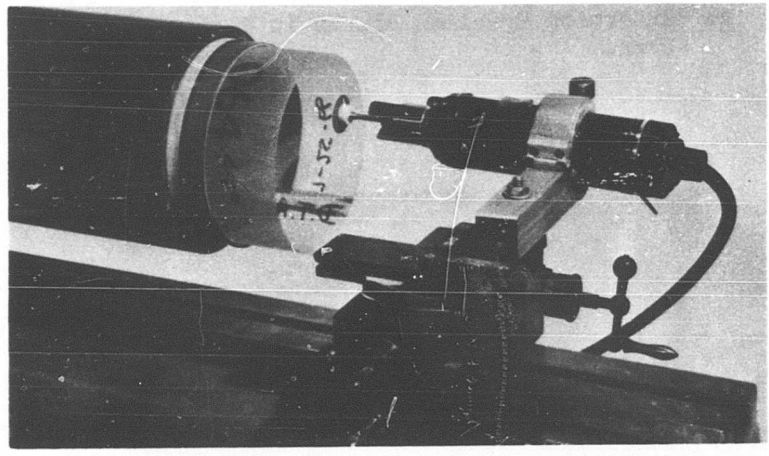

Figure 4. Trimming End of Specimen With Cutting Wheel.

SPECIMEN PREPARATION FOR TEST

Specimens, manufactured as described previously, were mounted in end plates for testing. The end plates consisted of a pair of aluminum disks machined to fit properly into place in the test machine, and grooved to accept the ends of the specimens. The grooves had an inside diameter of 4.755 inches, were $\frac{1}{2}$ inch deep, were 3/16 inch wide at the bottom, and had a 5^{o} relief on the outer wall to facilitate removal of specimens following testing. Close tolerances were maintained on the end plates to insure concentricity of the test machine and specimen when the latter was mounted for testing.

Consistency of end conditions was assured by potting the ends of the specimens into the end plate grooves using an epoxy resin. To maintain concentricity and parallelism of the end plates and specimen during this process, two potting jigs were used (Figure 5). The upper end plate was potted first, with the bottom of the specimen held by a spare upper end plate on the potting jig shaft. Then the specimen was turned over and potted into the lower end plate on a jig which had a raised portion concentric with the shaft, corresponding to the central cylinder of the test machine.

The potting medium used was an epoxy resin system consisting of 100 parts of Epon 828 resin to 30 parts of T-1 hardener. This mixture was easy to handle and cured rapidly in warm end plates. The end castings which resulted may be seen in Figure 11; a fully mounted specimen is shown in the test machine in Figure 10.

A silicone parting agent was used in the groove to facilitate removal of the specimens from the end plates after testing. Even with this precaution, some difficulty was experienced in removal. No specimen slipped in the end plates during testing.

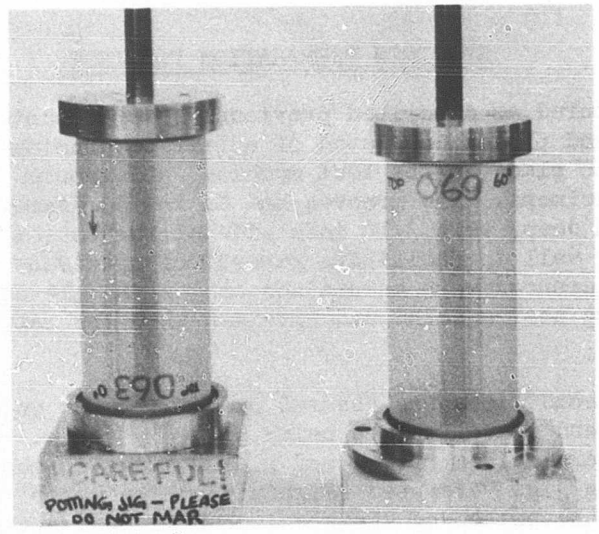

Upper End Plate Jig Lower End Plate Jig

Figure 5. Potting Jigs Used in Potting Specimens into End Plates.

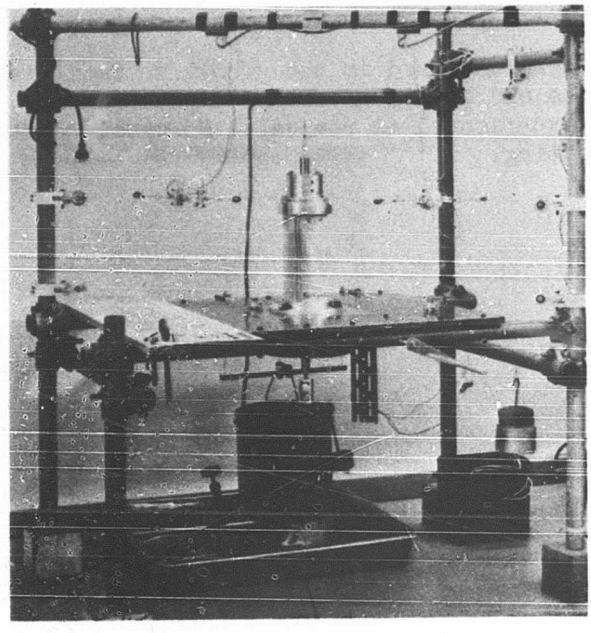

Figure 6. Test Machine in Operation (Note Buckled Specimen.)

DESCRIPTION OF THE TEST MACHINE

No test machine was available at Stanford University, or commercially, which could be used for this program. Therefore, it was necessary to design and construct a test machine. To avoid restricting the usefulness of the machine to a single project, the following capabilities were desired:

1. The machine should be capable of testing specimens of various sizes, initially cylindrical shells approximately 5 inches in diameter and 12 inches long.

2. The machine should be capable of loading the specimens in torsion, both clockwise and counterclockwise; in tension or compression; and in any combination of axial and torsional loadings.

3. Side loads and bending moments must be excluded, and the end plates must be maintained parallel to each other, but end shortening must be allowed.

A number of tests were made using a pilot model machine made of Dexion (pierced steel angle stock); on the basis of the performance of this machine, changes to the design were made where required.

The final result is the test machine shown in Figure 6. The specimen is restrained by the bottom end plate which is bolted to the table, and is loaded from the top. Torsion is applied by a couple acting on the loading heat pulley, and compression or tension forces are applied through the central shaft.

The table is a 3/4-inch steel plate, bolted to a frame of 2-inch steel tubing. The frame is joined with scaffolding pipe clamps. This clamping system leads to some lack of machine rigidity, but this was not considered to be important since it has already been demonstrated that test machine rigidity does not influence the initial buckling load for bodies.[9]

The central cylinder is mounted on a flat 12-inch square which was milled near the center of the table (Figure 7). This 4-inch outside diameter steel cylinder, machined to close tolerances, has a 2-inch-diameter axial bore; two Rotolin GPX-2 precision bearings are fitted in the bore, top and bottom. These bearings allow both rotation and translation of the central shaft, which runs in them. The massiveness and rigidity of the table-cylinder assembly insure that the operating centerline of the system is stable.

The loading head consists of a 5-inch-diameter pulley bolted to a 3-inch aluminum cylinder, all mounted on a 1-inch-diameter precision-ground steel shaft 2 feet in length and secured with taper pins. The length of the cylinder along the shaft insures that the pulley and table are parallel when the shaft is inserted in the bearings in the central cylinder. The torsional loading couple is applied to the pulley. Axial loads are introduced, and side loads are precluded by the central shaft.

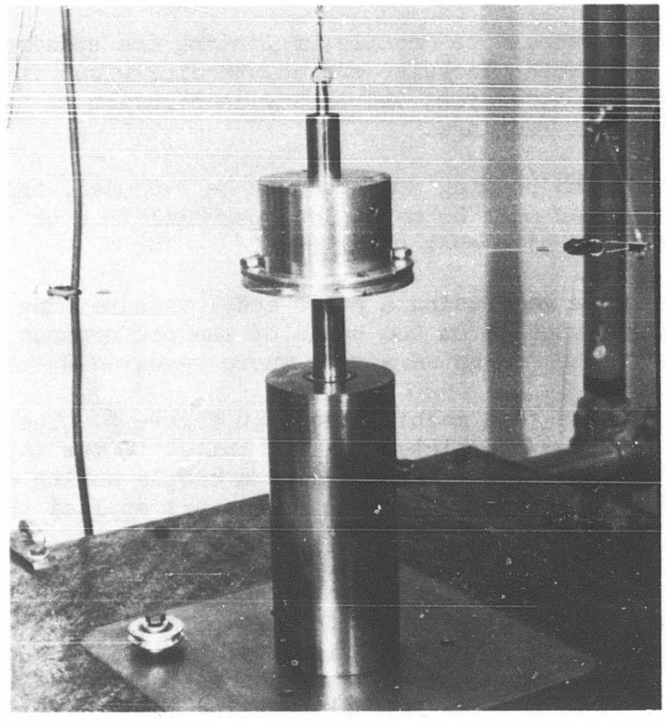

Figure 7. Test Machine, Central Cylinder, Central Shaft, and Loading Head.

It is clear from the work of Strum[10], Horton and Durham[11], and Horton and Cox[12] that, for cylindrical shells under external pressure, compression, or combined compression and flexure, if the extent of motion is restricted during the buckling process, repeated valid tests are possible on the same vehicle. In the above-referenced tests, the buckle restriction device was a closely fitting internal mandrel. However, the effect of initial buckling on the subsequent behavior of cylinders under torsion does not appear to be as important, as is evidenced by the fact that the buckles are of a diagonal tension field kind and initial imperfections appear to have a less deciding role in torsion behavior. Thus, although deflection limitation was considered to be essential in the test series, a more elementary process was followed: the extent of angular rotation rather than the buckle depth was restricted. The deflection limiter which accomplished this is clamped to the central shaft beneath the table (Figure 8). The device is a strong lever free to rotate between two adjustable stops. In all tests, the system was set to restrict the maximum angular rotation to between 1.5° and 2.5°.

The central shaft with all appurtenances fitted weighs 15 pounds. Since this deadweight would create, in essence, a compressive preload on the test vehicles, it is carefully counterbalanced.

Torsional loading is accomplished through a deadweight system in which the weight of water in a loading bucket is transferred through loading wires to the loading head. Axial loading, if required, could be accomplished similarly. Water is used as the load-producing medium since, by this means, very smooth action can be obtained. Rate of loading is easily varied. Adjustment of bucket location on the bucket beam equalizes tension in the wires. To eliminate the effects of wire stretching, the system was designed so that wire lengths are identical for the two load paths. Total load is controlled by an off-on solenoid valve in the water line, and loading rate is adjusted with a throttling valve.

To mount a specimen for test, the lower end plate is slid down the central cylinder to the table, the central shaft is inserted through the upper end plate and the Rotolin bearings, and the end plates are tightly bolted to the table and loading head. Close tolerances on fit between the central cylinder and lower end plate and between the upper end plate and the central shaft insure that the plates are parallel and concentric. The bolts attaching the end plates to the table and the loading head must be torqued down firmly. This insures that torsion is transferred through friction between end plates and table or head, rather than through bolt-thread contact; thus, the possibility of slippage during testing is reduced.

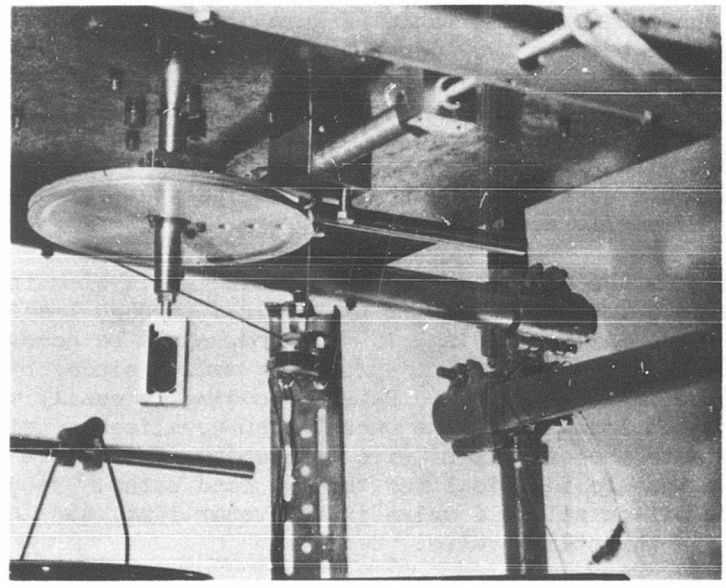

Figure 8. Test Machine - View Beneath Table Showing Deflection Limiter, Rotation Pulley and Potentiometer, and Rotation Mirror.

INSTRUMENTATION

TORSION MEASUREMENT

Torsion was applied to the loading head by a couple. The forces constituting this couple were carried to the application point through wires. The tension in the individual wires was measured at the loading head by a strain gage load link in each line (Figure 6). The links were gaged with Baldwin SR-4 wire strain gages, and they were used in conjunction with Sanborn Model 1100 carrier preamplifiers and a six-channel Sanborn Model 100BW pen recorder to provide a written record of tension in each wire. The links were dead-load calibrated; load determination accuracy was $\pm$ 0.5 pound, which corresponds to 2.5 pound-inch torque.

ROTATION MEASUREMENT

Rotation was measured in two ways. A gross reading, used to monitor the maximum rotation values, was obtained using a Fairchild No. 744 linear precision potentiometer, belt driven from a pulley attached to the deflection limiter clamp (Figure 8). This 10,000-ohm, $\pm$ 0.15-percent potentiometer was used as a voltage divider; 10-volt DC was supplied by a battery and the output was recorded using a Sanborn Model 1800 stabilized DC preamplifier and a six-channel recorder.

Fine measurement of rotation was accomplished using an optical lever system consisting of a transit, a 1/8 wave-length first-surface mirror, and a lighted meter stick (Figure 9). The mirror was attached to the bottom of the test machine central shaft (Figure 8). The operator sighted through the transit at the reflection of the meter stick in the mirror. Rotation of the shaft caused an apparent motion of the meter stick beneath the transit hairline with 1 millimeter of travel corresponding to 0.005° rotation. By means of the remote marker feature of the six-channel recorder, the operator marked the edge of the test record at each millimeter of travel during the early stages of a run. As the specimen approached failure, the rate of rotation accelerated, and marks were made every 5 millimeters, corresponding to 0.025° rotation, until failure occurred.

RADIAL DEFLECTION MEASUREMENT

Several tests were made during which radial deflection was measured using a Model KD-36 Fotonic Sensor, Figure 10, in conjunction with a Sanborn Model 1300 DC coupling preamplifier and the six-channel recorder. The Fotonic Sensor requires a flat, reflective surface at the point of measurement. This was provided by attaching a small square of Alzac foil to the specimen at the desired point with Duco cement.

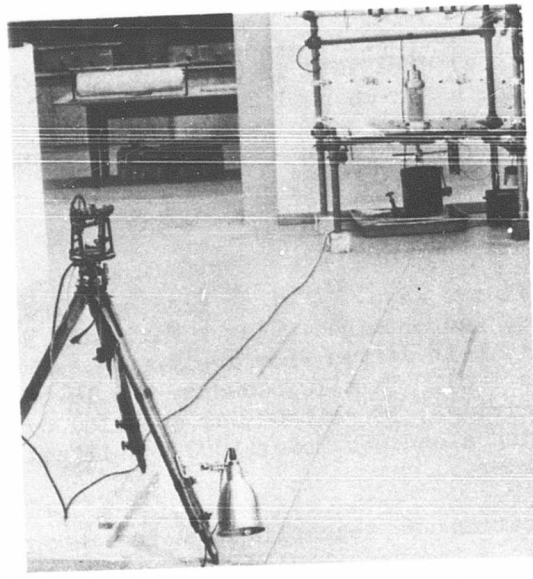

Figure 9. Test Machine - Optical Rotation Measurement System.

TEST PROCEDURE

Specimens were prepared and mounted in the test machine as described previously. Torsion was applied by running water into the bucket at a controlled rate until the specimen's rotation reached the limit value. Readings of tension in each load wire and angular rotation of the loading head were recorded throughout the test. Edges and centerlines of buckles and flutes on the failed specimen were marked with a felt pen. The water was drained from the bucket, and the specimen returned to its unbuckled configuration. Wires were reversed and a second test was made, twisting the specimen in the opposite direction, using the same procedure.

For Fotonic Sensor runs, the specimen was tested once as described above. A square of alzac foil was attached to the centerline of a buckle and the sensor was calibrated on that surface. The specimen was then tested again in the same direction as the first test, and Fotonic Sensor data, as well as the data mentioned above, were recorded. Finally, the specimen was tested in the opposite direction.

DISCUSSION OF RESULTS

Data from the various tests are presented in Table I. Fiber angle is the angle between the direction of the warp and the projection of the axis of the direction of the warp and the projection of the axis of the specimen on the surface; thus, in a 0° specimen the warp runs parallel to the axis, while in a 90° specimen the warp is circumferential. Weight and length of the cylinder were determined as described on page 5. θ_{crit} was computed from the difference between the initial transit reading and the reading after which the operator was unable to mark the rotation at 0.025° intervals. This point was clear cut; repeatability of this reading was such that readings on successive tests in the same direction were within 0.05° of each other. "Number of flutes" indicates the number of buckle flutes found on the cylinder circumferentially. T_{crit} is the critical torque; N_{crit} is the critical normalized torque parameter described in subsection "Buckle Patterns".

In most questions of instability of real structures, i.e., other than perfect vehicles, the definition of critical load value is fundamental but obscure. Admittedly, in the case of cylinders under axial compression or compression combined with other loadings, there is a distinct snap process and a subsequent load fall off; bodies under the action of external pressure are likewise characterized. The tube under torsion presents a more difficult assessment problem. There is not always a marked change in load-carrying capability when a buckle has begun to develop. Thus, for the tests other than those using the Southwell technique, it was necessary to define the state which was to be interpreted as critical. In the work reported, the state chosen was that at which it was no longer possible to determine, by a visual technique, the rotation as a function of torque. In essence, this approach corresponds to the "top of the knee" technique so frequently adopted for the plate. It must be emphasized that the critical level, so defined, does not correspond to the formation of the first buckle. Indeed, in a number of cases the specimen was visibly buckled by loads considerably less than T_{crit} so defined.

ADJUSTMENT FOR RESIN CONTENT

It was apparent during testing that maximum torque values were dependent to some extent on the weight of the specimen. To compensate for the variation due to weight, a "normalized torque parameter", the ratio of torque to specimen weight, was used. This ratio was chosen because, analytically, torsional strength is directly proportional to wall thickness, and wall thickness is directly proportional to specimen weight, at least to a first-order approximation. Standard deviations of critical normalized torque parameters were smaller than standard deviations for raw values of critical torque throughout the various categories considered, and distribution, as may be seen from a comparison of the histograms (Figure 12) and the probability plots (Figures 13-17). The normalization procedure was especially important in allowing comparison of groups of specimens where the mean weights of the groups differed considerably due to manufacturing technique, as between the 60° specimens and other groups.

TABLE I. CHARACTERISTICS OF TEST VEHICLES AND TEST DATA

Cyl No.	Fiber Angle (deg)	Wt. (gm)	Length (in)	Run	Direction	T_{cr} (lb-in)	θ_{cr} (deg)	N_{cr} (lb-in./gm)	No. of Flutes
001	90	31.8	10.75	1	cw	109.2	1.050	3.44	7
				2	ccw	118.2	.825	3.60	7
				3	cw	106.8	.950	3.36	7
				4	ccw	119.0	.745	3.75	7
				5	cw	104.5	.950	3.28	7
				6	ccw	116.2	.775	3.66	7
002	0	36.6	10.75	1	cw	110.2	.500	3.01	8
				2	cw	107.6	.500	2.94	8
				3	cw	105.0	.525	2.87	8
				4	ccw	114.5	.575	3.13	8
				5	ccw	105.3	.575	2.88	8
				6	ccw	105.5	.550	2.89	8
003	90	33.8	10.72	1	cw	118.0	.700	3.49	7
				2	ccw	130.2	.525	3.84	7
				3	cw	107.4	.700	3.18	7
				4	ccw	123.0	.500	3.64	7
				5	cw	102.8	.725	3.03	7
				6	ccw	125.0	.500	3.70	7
004	90	31.6	10.75	1	cw	103.0	.800	3.26	7
				2	ccw	116.5	.540	3.68	7
				3	cw	97.5	.700	3.08	7
				4	ccw	112.5	.530	3.56	7
				5	cw	96.2	.700	3.04	7
				6	ccw	111.5	.490	3.53	7
005	45	32.5	10.75	1	cw	88.0	.300	2.71	7
				2	ccw	85.6	.225	2.64	7
				3	cw	85.2	.275	2.62	7
				4	ccw	82.1	.225	2.52	7
				5	cw	82.5	.275	2.54	7
				6	ccw	81.2	.250	2.50	7
006	46	32.6	10.75	1	ccw	81.9	.400	2.51	7
				2	cw	90.1	.325	2.76	7
				3	ccw	77.5	.375	2.38	7
				4	cw	88.6	.275	2.72	7
				5	ccw	78.6	.375	2.41	7
				6	cw	87.0	.300	2.67	7
007	0	32.9	10.75	1	ccw	96.8	.725	2.94	8
				2	cw	83.5	.775	2.54	8
				3	ccw	91.5	.700	2.78	8
				4	cw	80.2	.700	2.44	8
				5	ccw	90.5	.675	2.75	8
				6	cw	73.2	.725	2.24	8

TABLE I - Continued

Cyl No.	Fiber Angle (deg)	Wt. (gm)	Length (in)	Run	Direction	T_{cr} (lb-in)	θ_{cr} (deg)	N_{cr} $\left(\frac{\text{lb-in}}{\text{gm}}\right)$	No. of Flutes
008	0	35.0	10.75	1	ccw	122.1	.725	3.49	8
				2	cw	106.9	.700	3.05	7
				3	ccw	115.6	.625	3.30	8
				4	cw	102.5	.700	2.93	7
				5	ccw	116.8	.600	3.33	8
				6	cw	101.6	.725	2.90	7
009	89	32.2	10.76	1	cw	100.0	.775	3.11	7
				2	ccw	96.9	.775	3.01	7
				3	cw	93.1	.825	2.90	7
				4	ccw	99.7	.750	3.10	7
				5	cw	92.1	.825	2.86	7
				6	ccw	95.8	.700	2.97	7
010	90	36.1	10.75	1	cw	126.2	.550	3.42	7
				2	ccw	147.5	.570	4.09	7
				3	cw	126.0	.550	3.49	7
				4	ccw	144.2	.500	4.00	7
				5	cw	123.5	.525	3.42	7
				6	ccw	145.0	.525	4.02	7
011	43	34.5	10.75	1	cw	99.5	.375	2.88	7
				2	ccw	92.5	.425	2.68	7
				3	cw	97.1	.400	2.82	7
				4	ccw	93.2	.400	2.70	7
012	44	33.8	10.75	1	cw	107.5	.200	3.18	7
				2	cw	108.4	.200	3.21	7
				3	ccw	100.2	.175	2.96	8
013	1	36.5	10.72	1	cw	117.4	.600	3.47	8
				2	ccw	130.0	.450	3.84	8
014	1	35.0	10.77	1	cw	106.6	.475	3.04	8
				2	ccw	123.5	.500	3.53	8
015	29	35.8	10.75	1	cw	132.5	.255	3.70	8
				2	ccw	106.7	.300	2.98	8
016	31	34.3	10.75	1	cw	90.5	.275	2.64	7
				2	cw	84.4	.275	2.46	7
				3	cw	84.5	.275	2.46	7
				4	ccw	102.5	.225	2.99	8
017	90	32.4	10.75	1	ccw	114.2	.725	3.53	7
				2	ccw	108.2	.650	3.34	7
				3	ccw	106.5	.650	3.28	7
				4	cw	116.5	.575	3.60	8
018	89	32.2	10.75	1	ccw	118.7	.725	3.69	7
				2	cw	109.5	.650	3.40	7

TABLE I - Continued

Cyl No.	Fiber Angle (deg)	Wt. (gm)	Length (in)	Run	Direction	T_{cr} (lb-in)	θ_{cr} (deg)	N_{cr} $\left(\frac{\text{lb-in.}}{\text{gm}}\right)$	No. of Flutes
019	0	32.3	10.75	1	ccw	104.2	.500	3.23	8
				2	cw	86.2	.800	2.67	8
020	1	33.7	10.78	1	ccw	106.0	.650	3.28	8
				2	cw	106.0	.525	3.28	8
022	42	31.5	10.75	1	ccw	96.5	.200	3.06	7
				2	cw	81.7	.225	2.59	8
023	29	31.2	10.75	1	ccw	94.0	.275	3.01	8
				2	cw	78.0	.250	2.5	7
024	30	33.8	10.75	1	cw	89.1	.300	2.64	7
				2	ccw	103.8	.275	3.07	7
025	89	31.9	10.75	1	cw	113.8	.550	3.57	7
				2	ccw	117.5	.600	3.68	7
026	90	33.2	10.75	1	ccw	128.0	.550	3.86	7
				2	cw	117.2	.600	3.56	7
027	42	33.4	10.75	1	cw	93.8	.350	2.81	7
				2	ccw	100.0	.325	2.99	7
029	0	35.1	10.76	1	cw	104.0	.500	2.96	7
				2	ccw	117.5	.450	3.35	8
030	1	32.3	10.75	1	cw	87.0	.550	2.69	7
				2	ccw	91.0	.625	2.82	7
031	29	31.2	10.75	1	cw	71.2	.375	2.28	7
				2	ccw	86.6	.400	2.78	7
032	30	32.0	10.76	1	cw	81.8	.350	2.56	7
				2	ccw	94.2	.450	2.95	8
033	61	31.1	10.75	1	cw	76.8	.325	2.47	8
				2	cw	73.9	.300	2.38	8
				3	ccw	105.0	.525	3.38	7
034	60	31.2	10.75	1	cw	77.2	.400	2.47	7
				2	ccw	101.5	.425	3.26	7
035	89	35.3	10.75	1	cw	134.8	.475	3.82	7
				2	ccw	138.5	.450	3.93	7
036	90	34.2	10.75	1	cw	107.2	.700	3.14	7
				2	ccw	121.0	.475	3.52	8
037	89	32.5	10.73	1	ccw	119.2	.650	3.67	7
				2	cw	121.2	.600	3.73	7
038	89	34.4	10.76	1	cw	115.8	.500	3.36	7
				2	ccw	112.5	.600	3.27	7
039	45	33.2	10.75	1	cw	99.5	.165	3.00	7
				2	ccw	102.0	.175	3.07	7
040	45	34.3	10.75	1	cw	109.8	.175	3.20	7
				2	ccw	104.2	.225	3.04	7
041	0	33.2	10.75	1	cw	100.0	.500	3.01	8
				2	ccw	104.5	.575	3.15	7

TABLE I - Continued

Cyl No.	Fiber Angle (deg)	Wt. (gm)	Length (in)	Run	Direction	T_{cr} (lb-in)	θ_{cr} (deg)	N_{cr} $\left(\frac{\text{lb-in.}}{\text{gm}}\right)$	No. of Flutes
042	0	32.7	10.75	1	ccw	111.5	.475	3.41	8
				2	cw	104.2	.425	3.19	8
043	60	30.9	10.76	1	ccw	113.5	.325	3.68	7
				2	cw	74.0	.250	2.40	7
044	60	31.9	10.75	1	cw	84.2	.225	2.64	8
				2	ccw	112.2	.325	3.52	7
045	90	32.6	10.75	1	cw	124.8	.500	3.83	7
				2	ccw	120.0	.495	3.68	7
046	0	32.7	10.75	1	cw	126.5	.525	3.87	7
				2	ccw	125.5	.525	3.84	7
047	45	34.1	10.75	1	cw	97.5	.375	2.86	7
				2	ccw	95.5	.300	2.80	7
048	45	34.3	10.75	1	cw	94.8	.250	2.76	7
				2	ccw	95.5	.300	2.78	7
049	0	32.6	10.75	1	ccw	106.8	.400	3.27	8
				2	ccw	108.8	.425	3.33	8
				3	cw	108.0	.400	3.31	8
050	1	31.9	10.75	1	cw	92.5	.575	2.90	8
				2	ccw	88.0	.625	2.76	7
051	90	31.3	10.75	1	cw	103.2	.775	3.30	7
				2	ccw	101.0	.675	3.23	7
052	0	31.7	10.75	1	ccw	117.0	.625	3.69	7
				2	cw	109.5	.625	3.46	7
053	44	33.2	10.75	1	ccw	90.0	.225	2.71	8
				2	cw	104.0	.175	3.13	7
054	44	32.7	10.73	1	cw	100.2	.425	3.06	7
				2	ccw	89.8	.225	2.75	7
055	1	33.5	10.75	1	cw	102.8	.500	2.91	8
				2	ccw	104.8	.575	2.97	8
056	0	32.9	10.76	1	cw	89.5	.625	2.72	8
				2	ccw	98.2	.575	2.99	8
057	45	33.2	10.76	1	ccw	91.2	.175	2.75	7
				2	cw	105.2	.200	3.17	7
058	45	35.0	10.75	1	cw	109.5	.425	3.13	7
				2	ccw	97.0	.350	2.77	7
059	1	33.0	10.75	1	cw	94.8	.600	2.87	8
				2	ccw	115.2	.475	3.50	8
060	0	33.8	10.75	1	cw	106.2	.500	3.14	8
				2	ccw	119.8	.450	3.54	8
061	89	32.6	10.75	1	cw	115.2	.800	3.54	7
				2	ccw	122.5	.700	3.76	7
062	89	35.2	10.75	1	cw	127.9	.725	3.63	7
				2	ccw	122.5	.750	3.48	7

TABLE I - Continued

Cyl No.	Fiber Angle (deg)	Wt. (gm)	Length (in)	Run	Direction	T_{cr} (lb-in)	θ_{cr} (deg)	N_{cr} $\left(\frac{\text{lb-in.}}{\text{gm}}\right)$	No. of Flutes
069	60	29.8	10.75	1	cw	69.8	.400	2.34	8
				2	cw	66.5	.375	2.23	8
				3	cw	66.8	.325	2.74	8
				4	ccw	102.0	.495	3.39	7
070	60	32.6	10.75	1	ccw	112.5	.375	3.45	7
				2	cw	86.8	.200	2.66	7
072	90	31.4	10.75	1	cw	106.8	.500	3.40	7
				2	cw	102.5	.550	3.27	7
				3	cw	98.0	.550	3.12	7
				4	ccw	123.2	.550	3.93	7
MU	30	31.2	10.75	1	cw	94.2	.275	3.02	8
				2	cw	90.6	.300	2.90	8
				3	ccw	71.0	.225	2.28	7

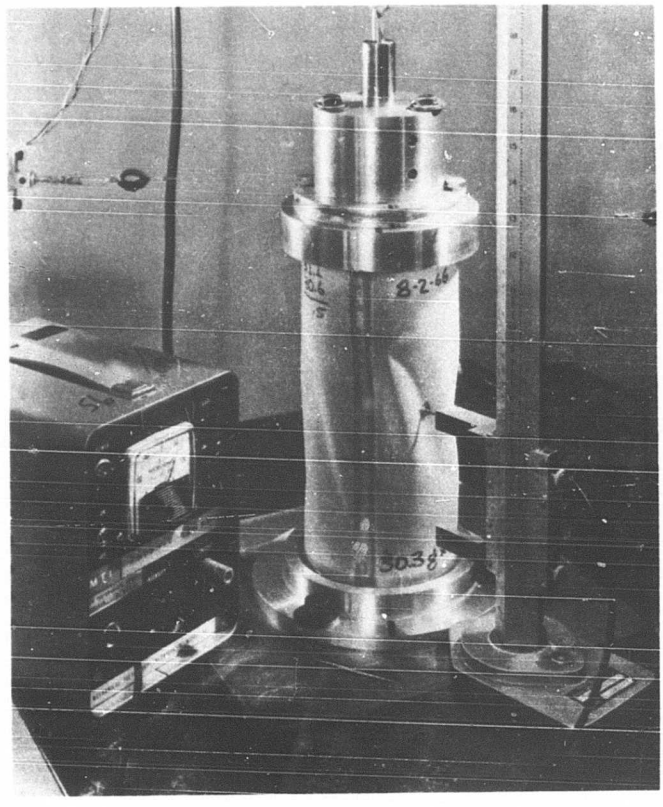

Figure 10. Test Machine - Radial Deflection Measurement Using Fotonic Sensor. (Note Alzac Foil Square Glued to Cylinder on Centerline of Buckle at Point of Measurement.)

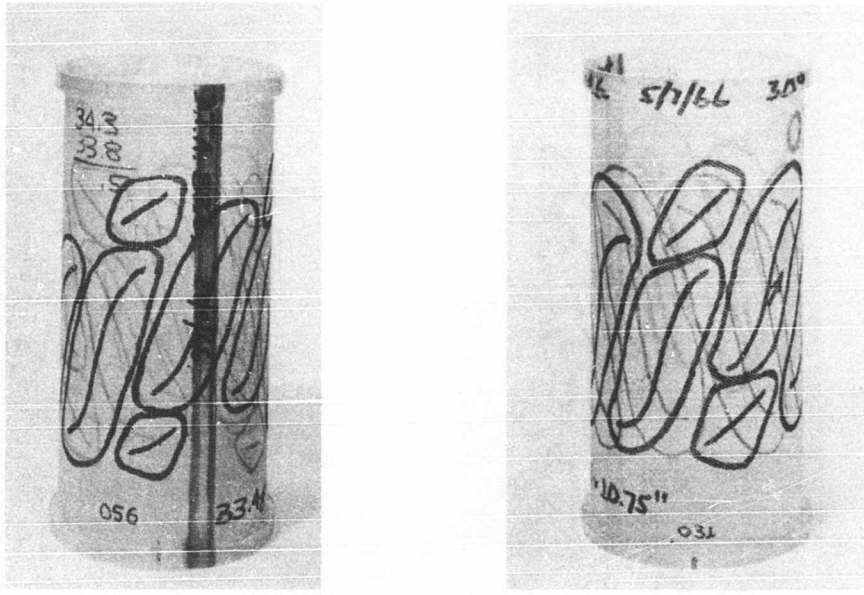

a. Cylinder 056, 0°

b. Cylinder 031, 30°

Figure 11. Typical Forsional Buckle Patterns Found in Open-Weave Single-Layer Fiberglass Specimens of Indicated Fiber Direction Groups.

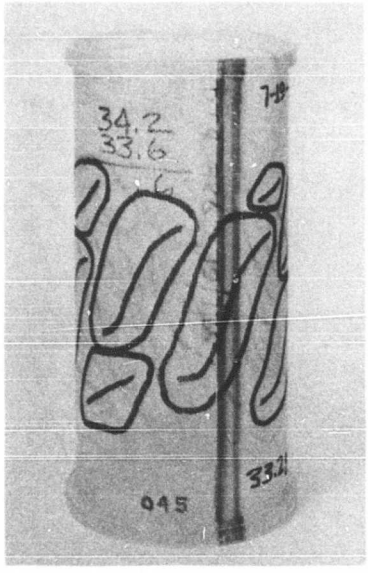

c. Cylinder 054, 45°

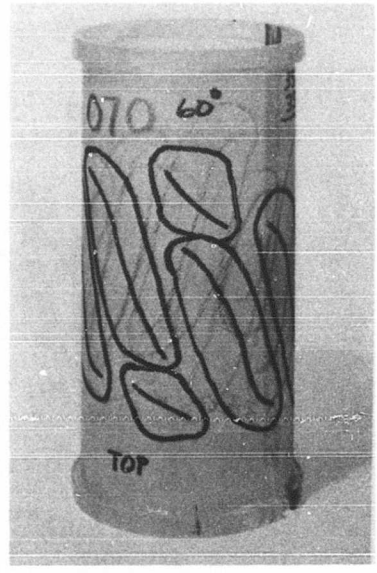

d. Cylinder 070, 60°

Figure 11. Continued.

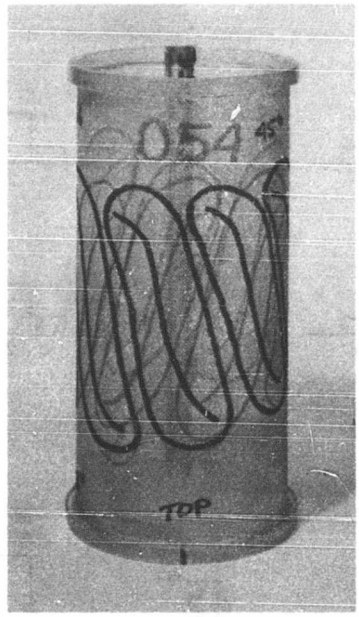

e. Cylinder 045, 90°

Figure 11. Continued.

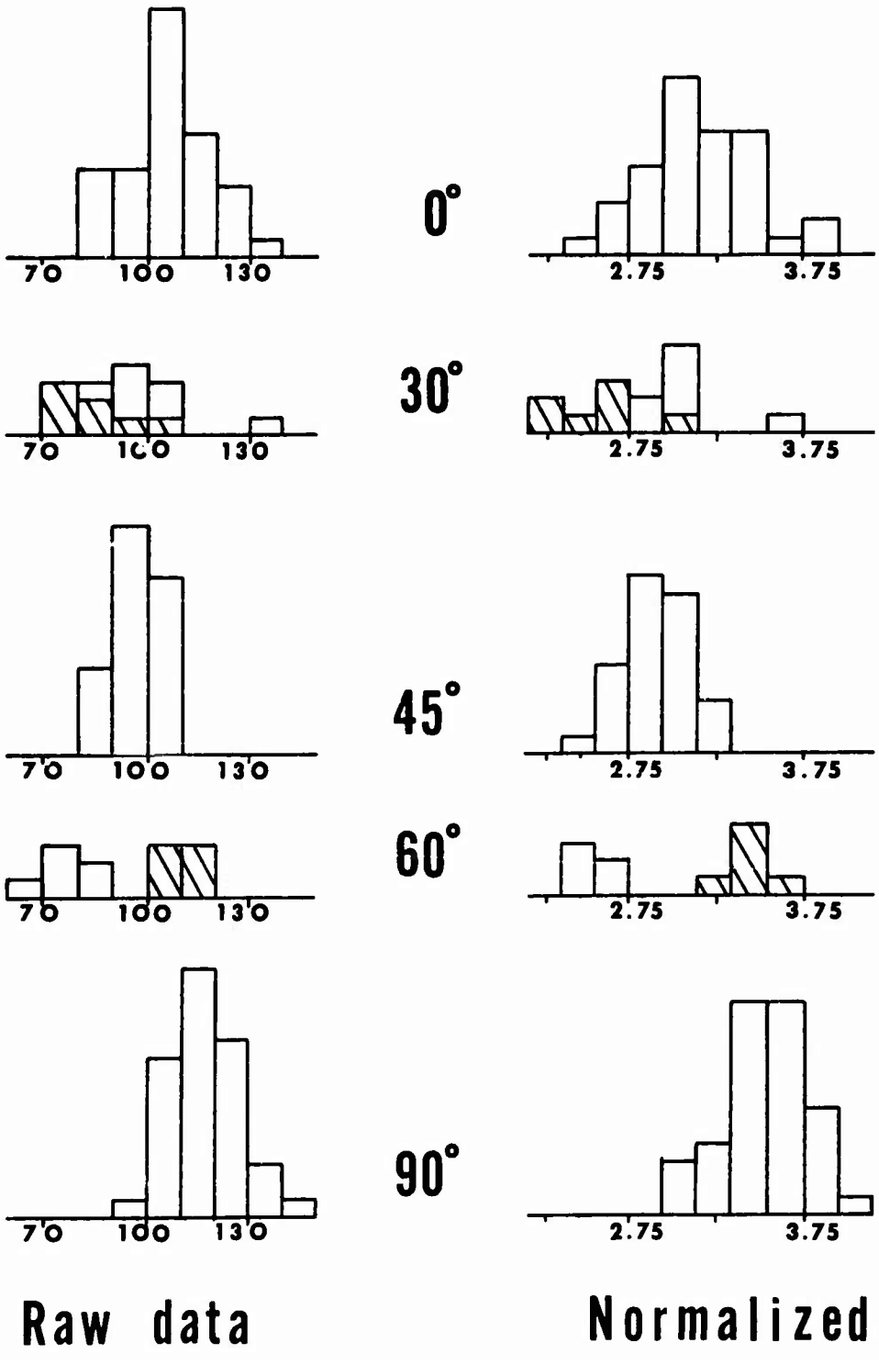

a. Frequency Distribution of Critical Torques and Critical Normalized Torque Parameters.

Figure 12. Frequency Distributions.

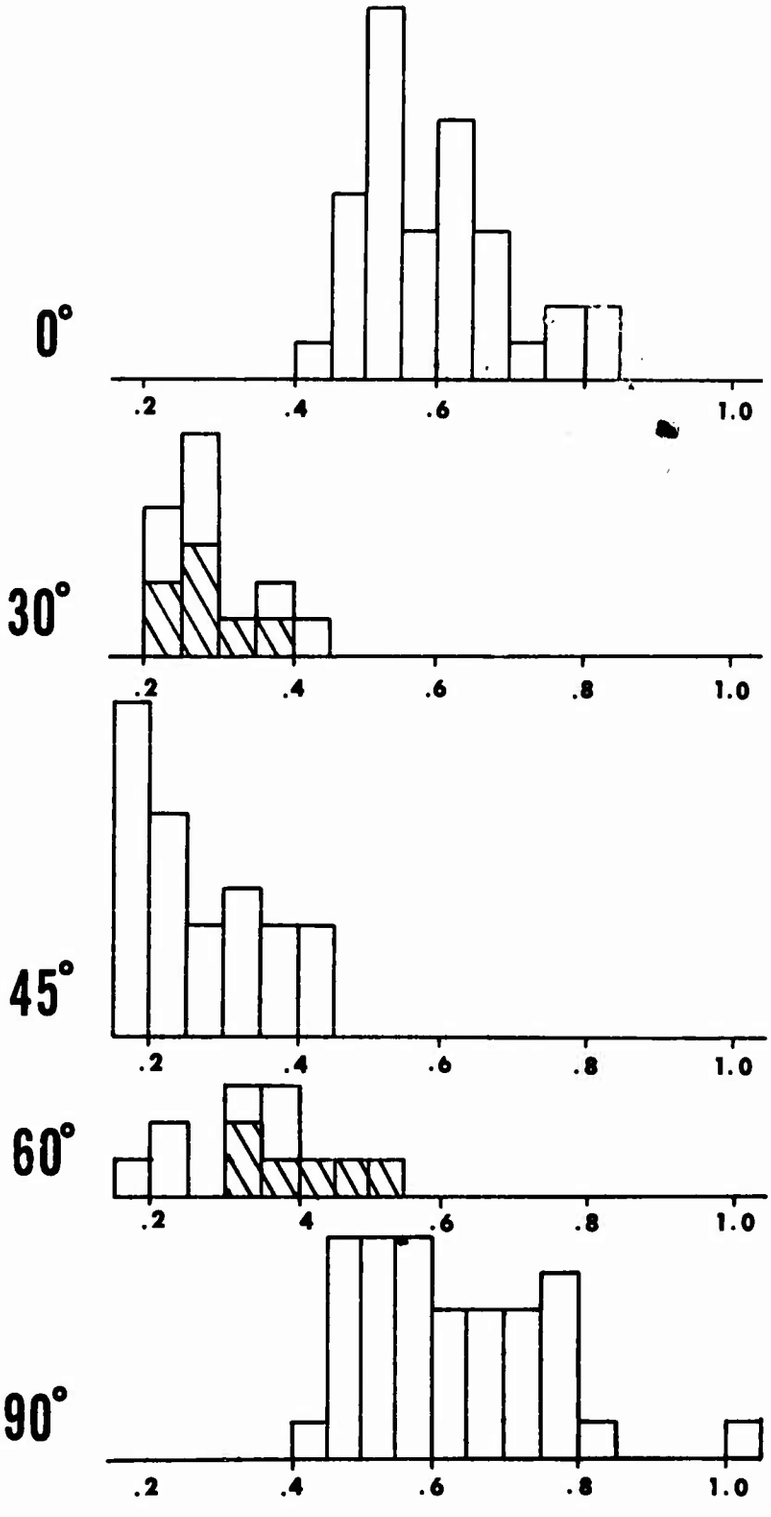

b. Frequency Distribution of Critical Rotation Angles.

Figure 12. Continued.

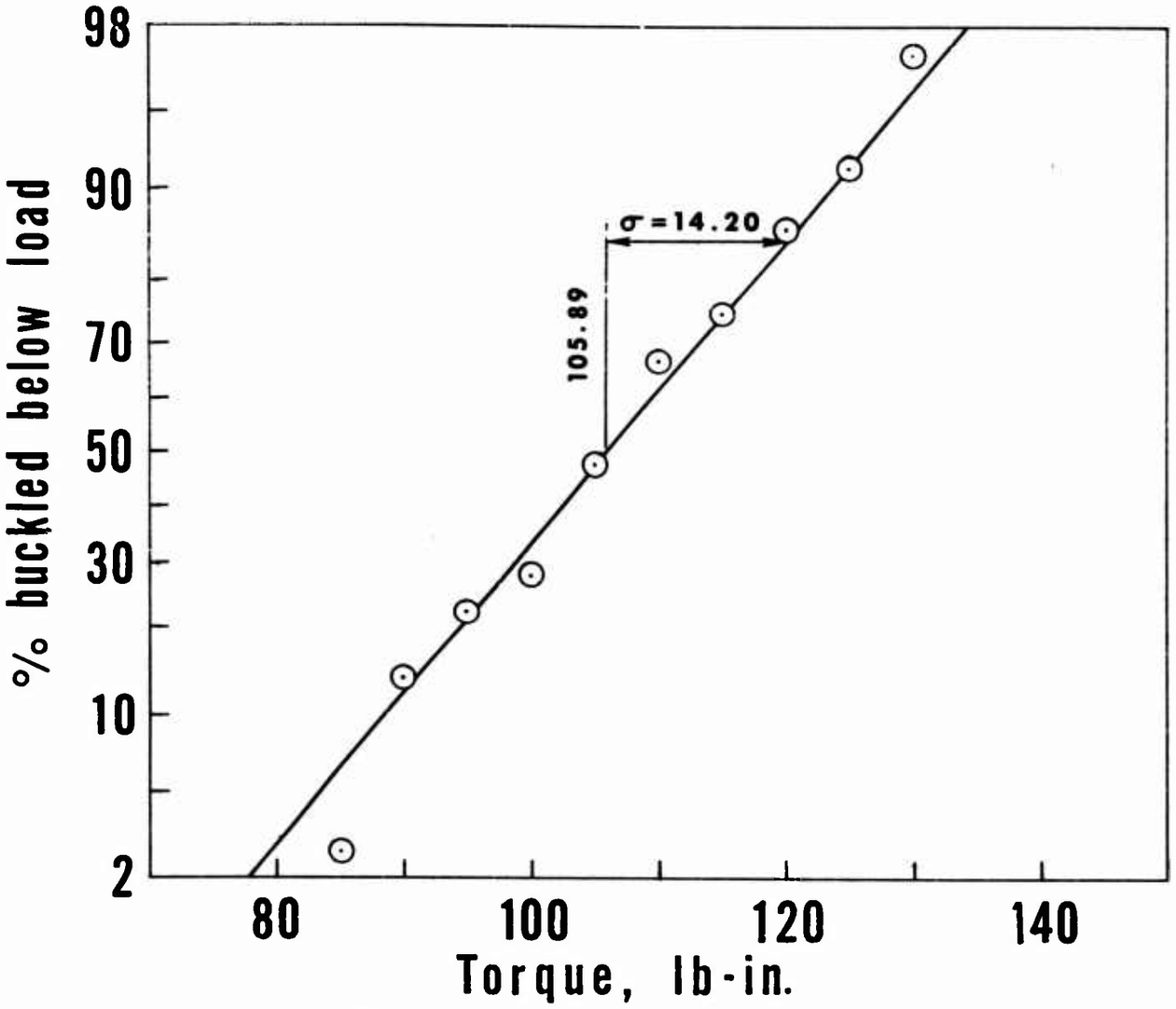

Figure 13(a). Probability Plots of Critical Torque.

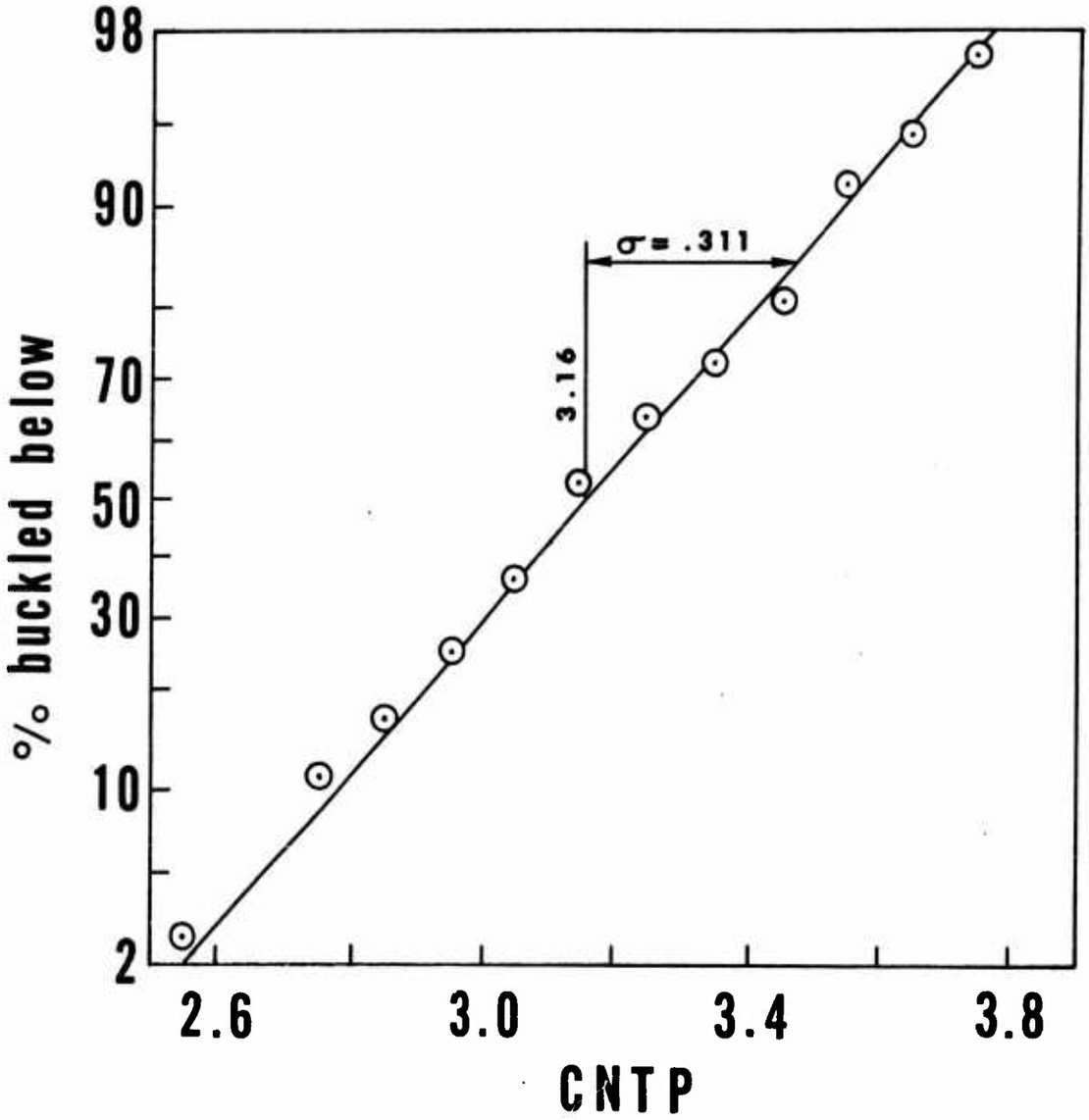

Figure 13(b). Probability Plots of Critical Normalized Torque Parameter (CNTP) for 0° Fiber Direction Group.

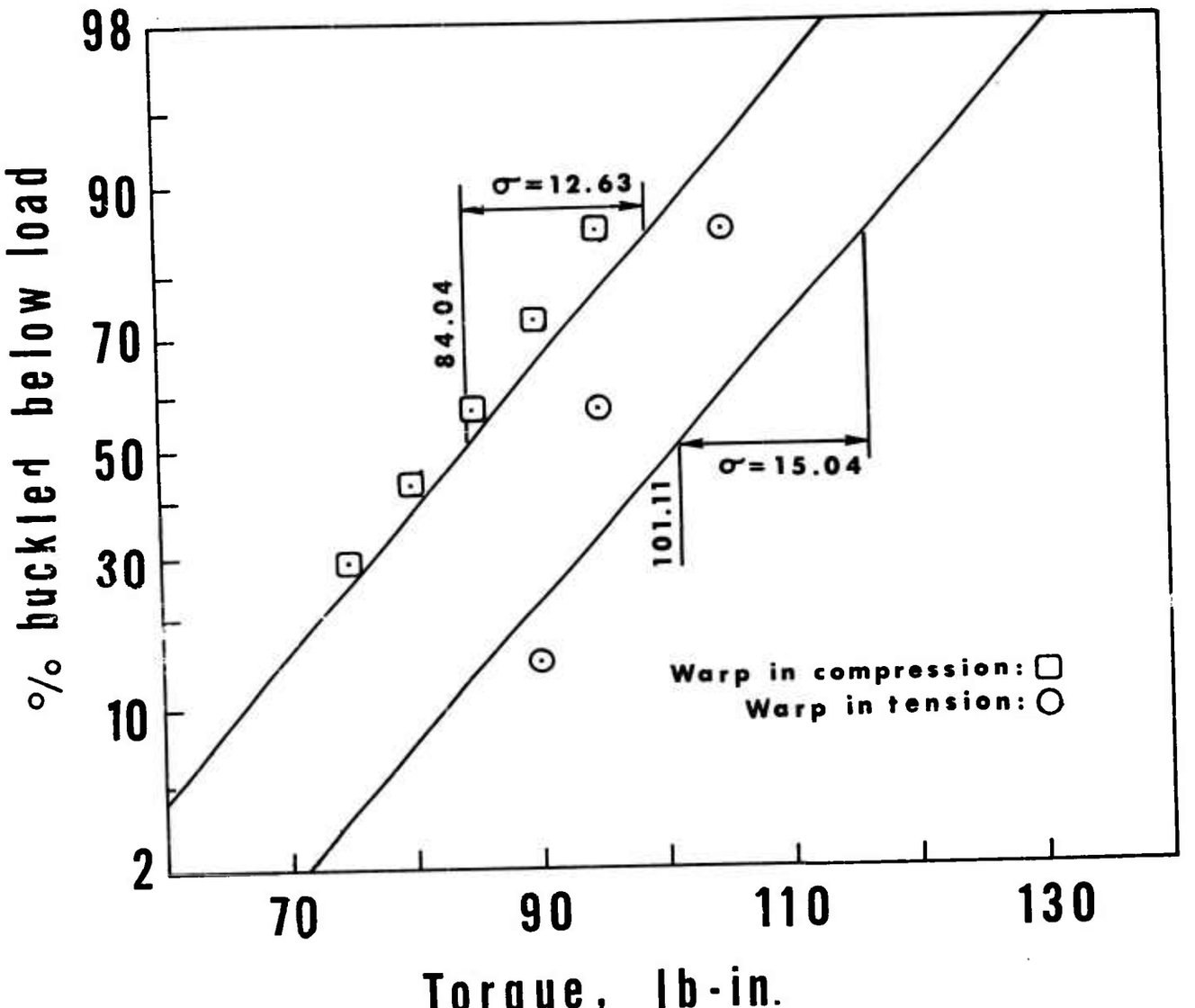

Figure 14(a). Probability Plots of Critical Torque.

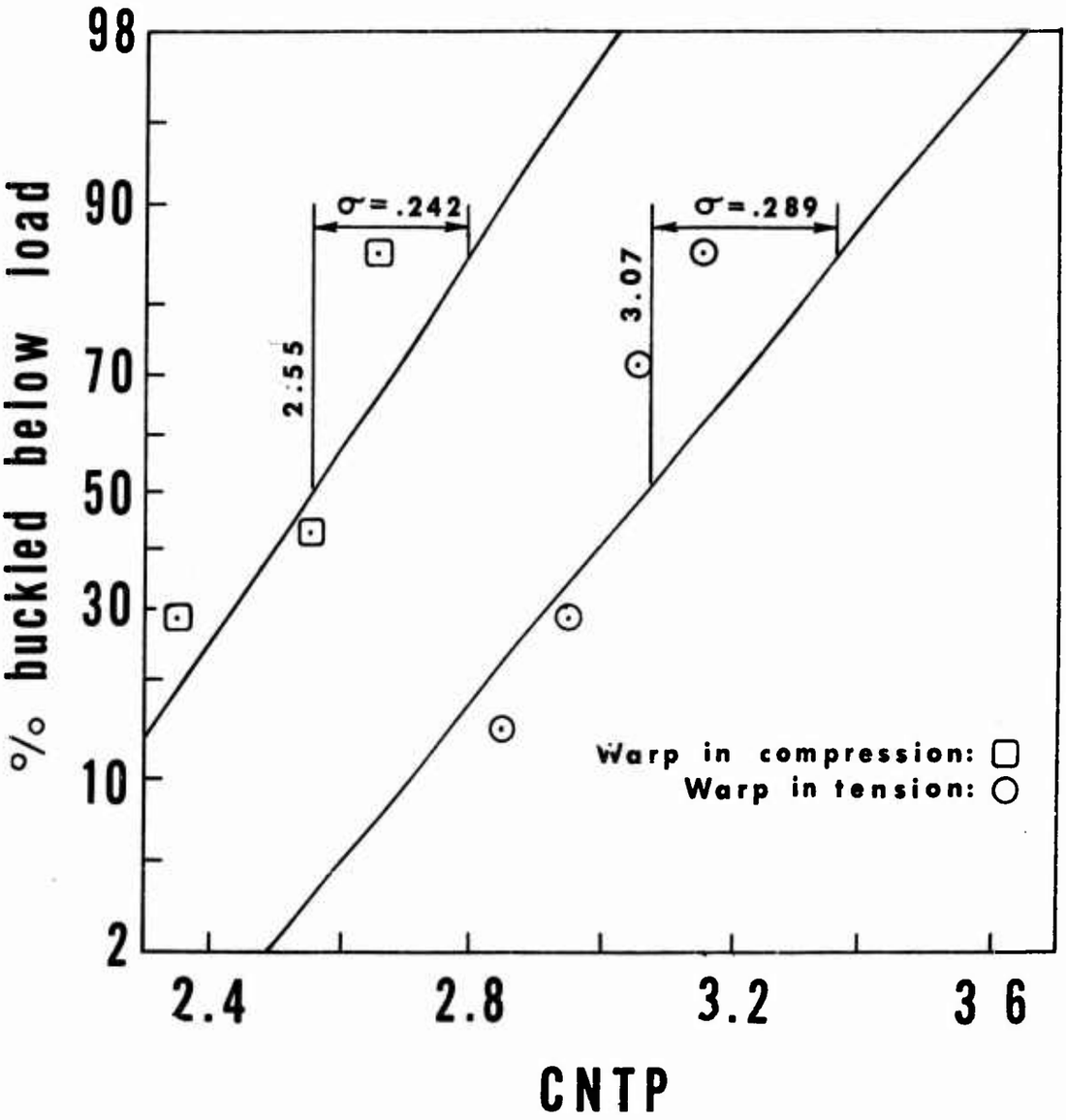

Figure 14 (b). Probability Plots of Critical Normalized Torque Parameter (CNTP) for 30° Figer Direction Group.

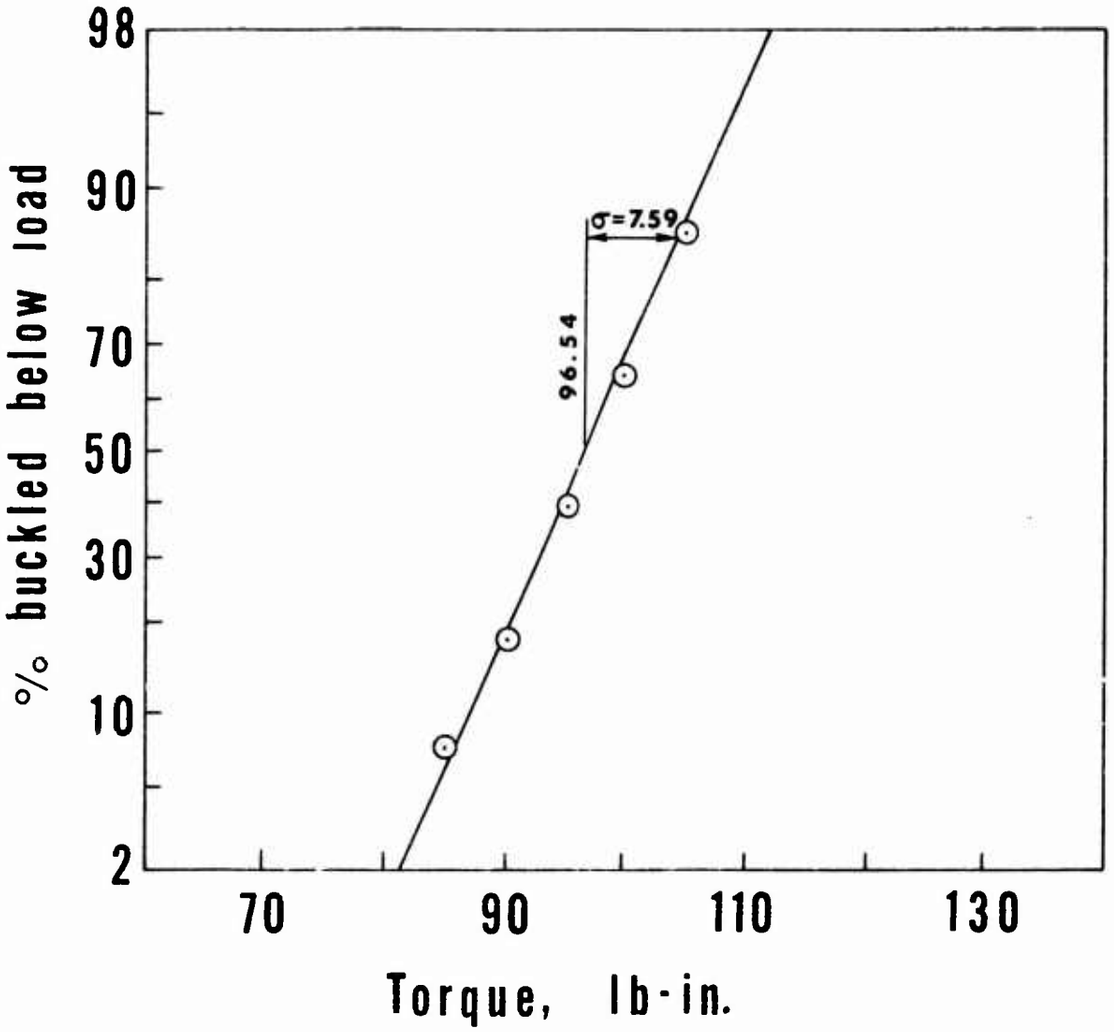

Figure 15(a). Probability Plots of Critical Torque.

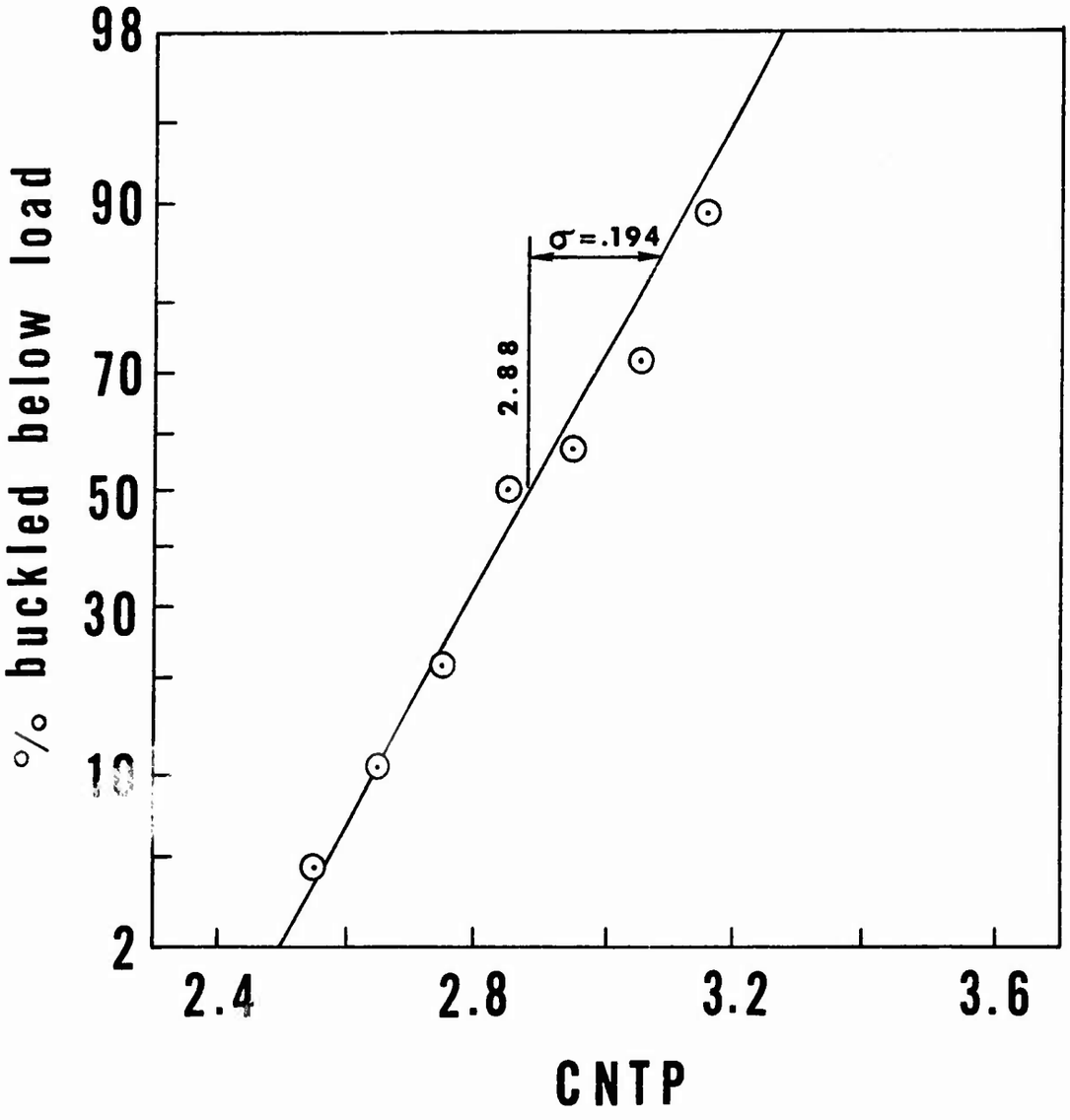

Figure 15 (b). Probability Plots of Critical Normalized Torque Parameter (CNTP) for 45° Fiber Direction Group.

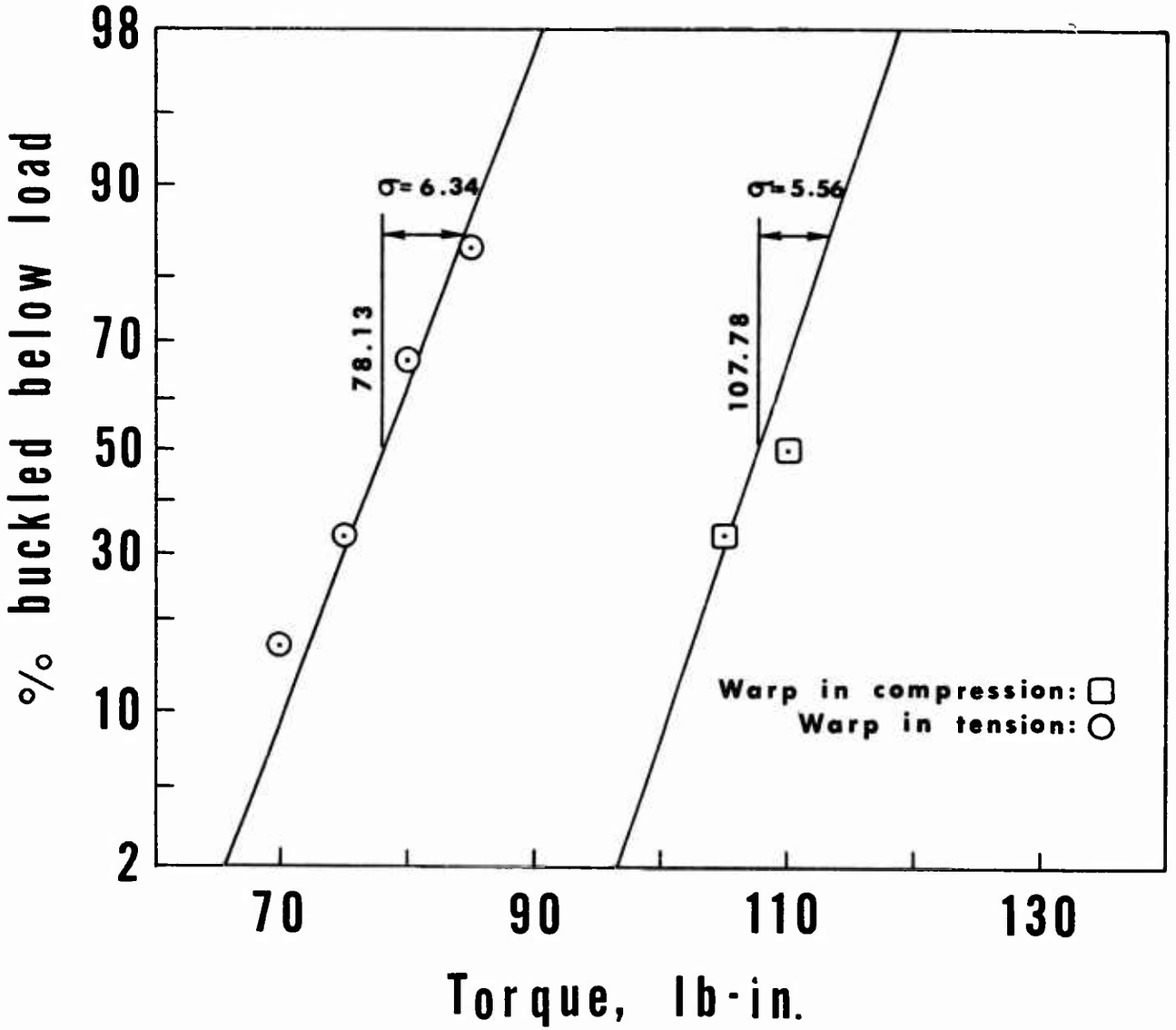

Figure 16 (a). Probability Plots of Critical Torque.

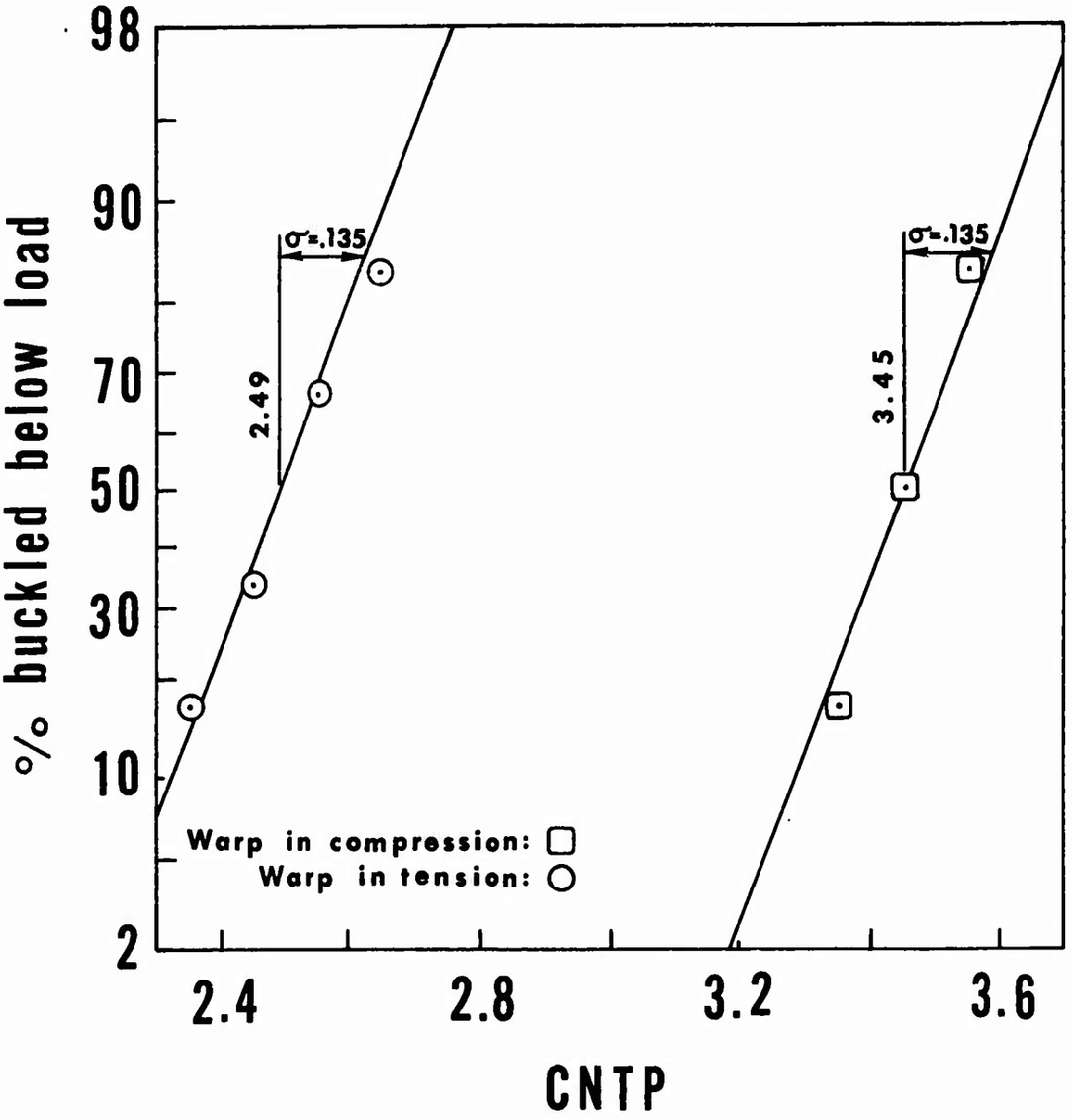

Figure 16 (b). Probability Plots of Critical Normalized Torque Parameter (CNTP) for 60° Fiber Direction Group.

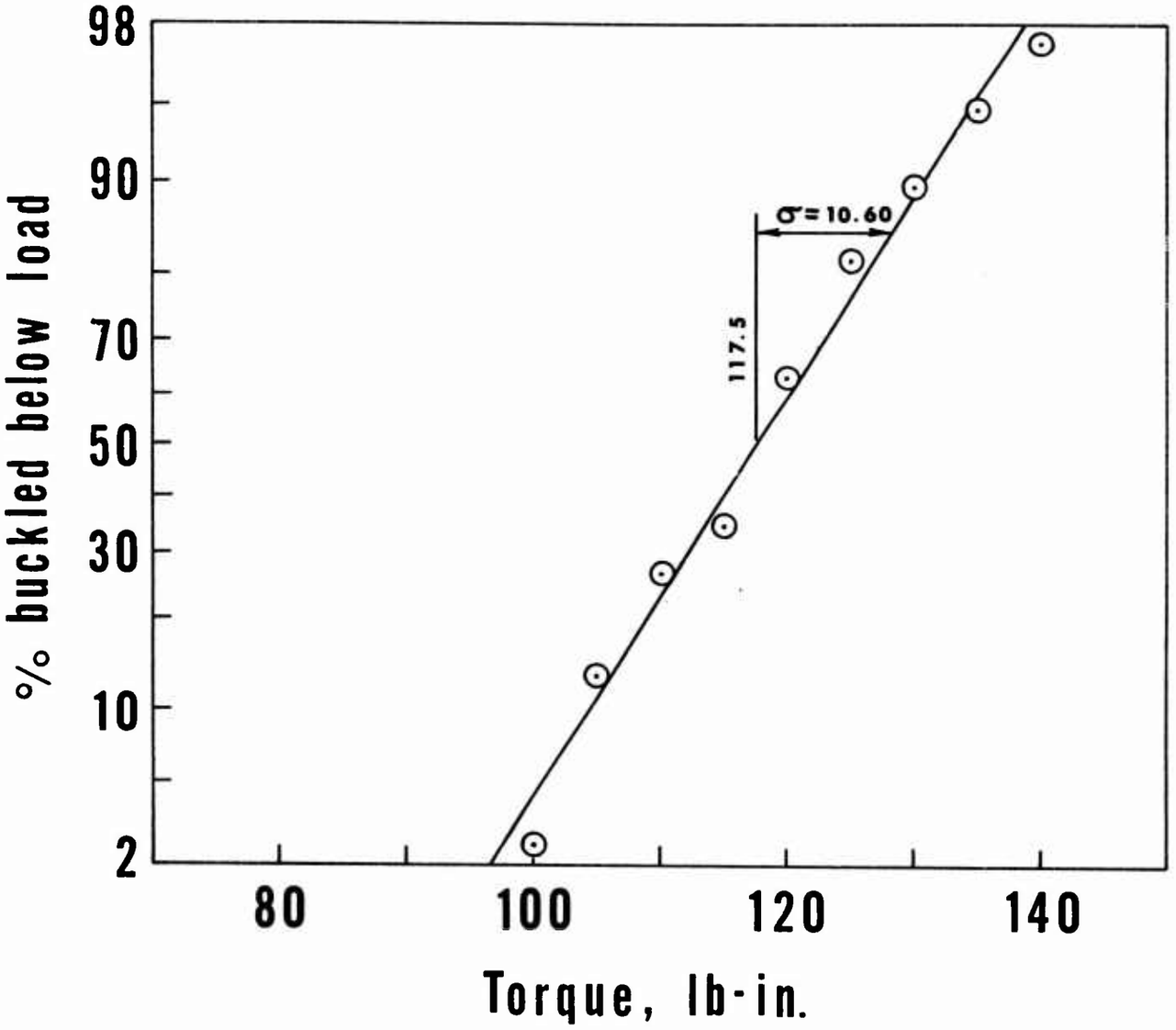

Figure 17 (a). Probability Plots of Critical Torque.

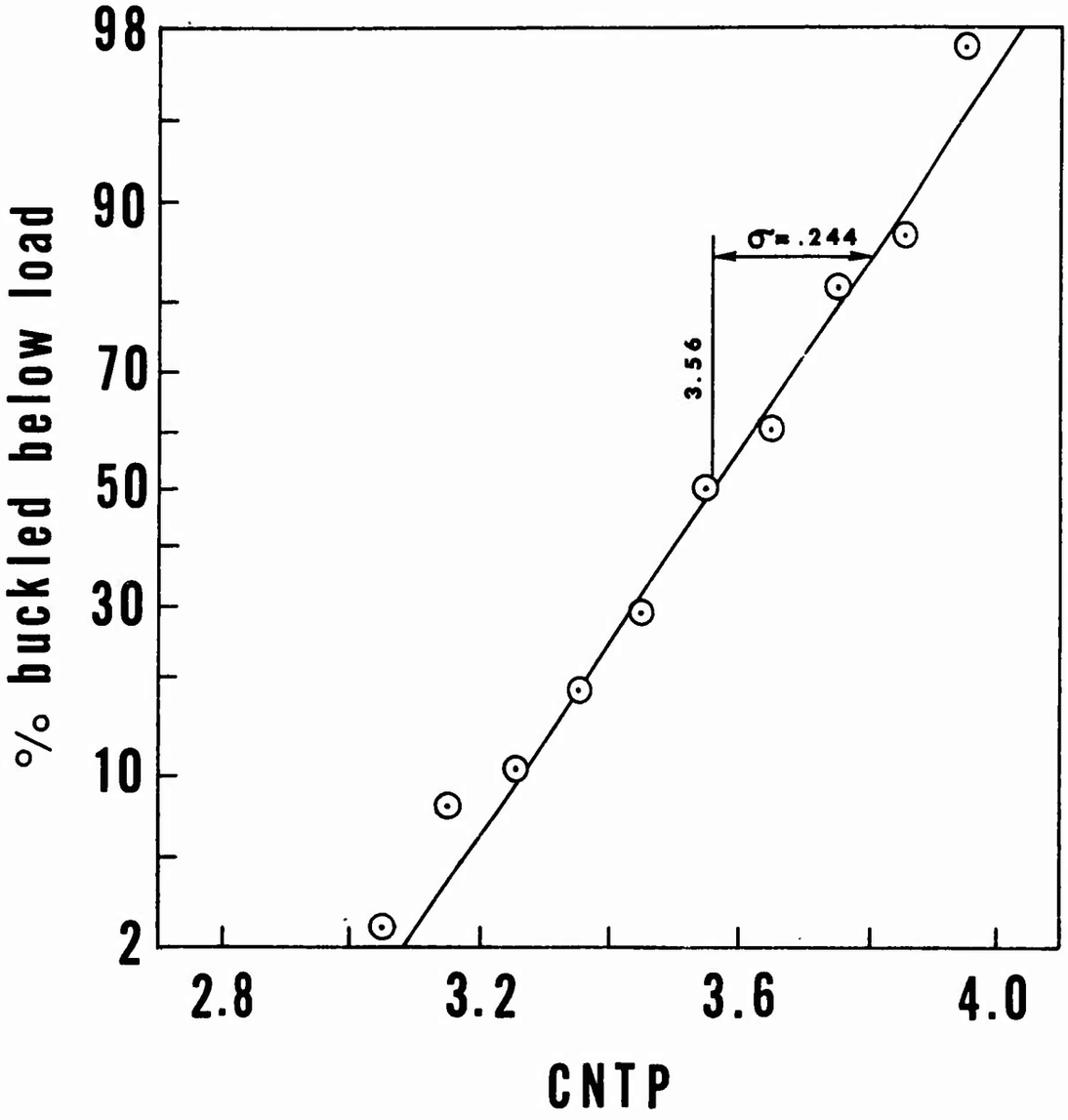

Figure 17(b). Probability Plots of Critical Normalized Torque Parameter (CNTP) for 90° Fiber Direction Group.

BUCKLE PATTERNS

All specimens developed buckle patterns consisting of either seven or eight inclined buckle flutes when sufficient relative rotation of the end plates was allowed (Figure 11). When rotation was stopped at a small value, between 1.5° and 2°, it was seen that these flutes were initially formed as an inclined row of diamond-shaped torsional buckles, which became a flute as they deepened with increasing rotation. Centerlines of the fully developed buckle flutes had an "S" shape, as upper and lower extremities curved to conform with the direction of the centerlines of the original diamond buckles. Deflection limiter settings used during testing generally resulted in stopping the relative rotation with the flutes only partially developed; however, in the case of the 45° specimens the flutes developed rapidly and completely. Ridge lines were generally quite well defined in the vicinity of the ends of the flutes; they were less well defined elsewhere. Again, 45° specimens were an exception: their flutes were smoother and less well defined throughout.

Table II shows the incidence of seven and eight buckle flutes by fiber direction groups. Seven flutes were predominant in all fiber direction groups except 0°; the 0° specimens buckled into eight flutes more often than seven. All groups had at least two specimens which buckled into eight flutes. Sixteen specimens buckled into seven flutes when twisted in one direction and into eight flutes when twisted in the other direction. Once the number of flutes had been established in a given direction, it remained the same for further tests in that direction. Individual diamond buckles appeared in different locations in the flute, but the number of flutes did not change, and the location of the flute centerline changed only slightly.

TORSIONAL STRENGTH AND RIGIDITY

A comparison of the mean critical normalized torque parameters for the five fiber angles tested is shown in Figure 18 and Table III; a comparison of the mean critical rotation angles is shown in Figure 19 and Table III.

Specimens with a 90° fiber orientation were the strongest and least rigid, while the 45° specimens were the most rigid and, with the exception noted below, the weakest. Thus, the specimens which carried the greatest load also absorbed the most energy.

The exception to this rule was found in the 30° and 60° specimens. As might be expected, the critical torque for these specimens depended on the direction of the applied torque. A much greater torsional load was carried in the "strong direction" (i.e., the direction in which the warp was in tension for the 30° specimens and in compression for the 60° specimens) than was carried in the "weak direction". In their strong direction, the mean critical normalized torque parameters for the 30° and 60° specimens approached the values for the 0° and 90° specimens, respectively. In their weak direction, the 30° and 60° specimens had mean critical normalized torque parameters lower than that for the 45° specimens. In addition, the 30° and 60° specimens were more rigid in their strong, rather than their weak, direction.

TABLE II. INCIDENCE OF SEVEN OR EIGHT BUCKLE FLUTES BY FIBER DIRECTION GROUPS

Number of Tests in which Flutes Numbered	Fiber Direction Group				
	0°	30°	45°	60°	90°
7	8	8	25	9	36
8	28	6	3	3	2

TABLE III. MEAN CRITICAL NORMALIZED TORQUE PARAMETERS AND MEAN CRITICAL ROTATION ANGLES BY FIBER DIRECTION GROUPS

	Fiber Direction Group					
	0°	30°		45°	60°	90°
MCNTP	3.16	3.07	2.55	2.88	3.45	2.49	3.56
θ_{cr}	.555	.308	.296	.275	.412	.300	.638

TABLE IV. RESULTS OF SPECIAL TESTS LEADING TO SOUTHWELL PLOT

Cyl. No.	Fiber Angle (deg)	Wt. (gm)	T_{cr} (lb-in.)	Southwell Slope (lb-in.)	Southwell Slope Normalized $\left(\frac{\text{lb-in.}}{\text{gm}}\right)$
002	0	36.6	107.6	106.3	2.91
MU	30	31.2	90.6	70.2	2.25
065	45	33.0	105.0	83.5	2.53
E	53	29.2	81.0	84.5	2.89
069	60	29.8	66.8	66.3	2.22
072	90	31.4	98.0	93.3	2.94

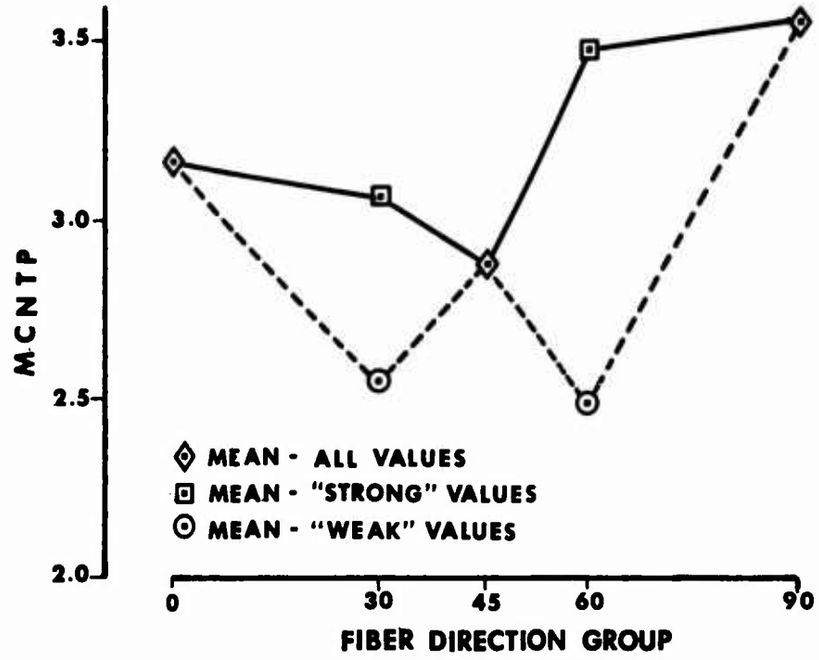

Figure 18. Mean Critical Normalized Torque Parameter (MCNTP) Variation With Fiber Direction Group.

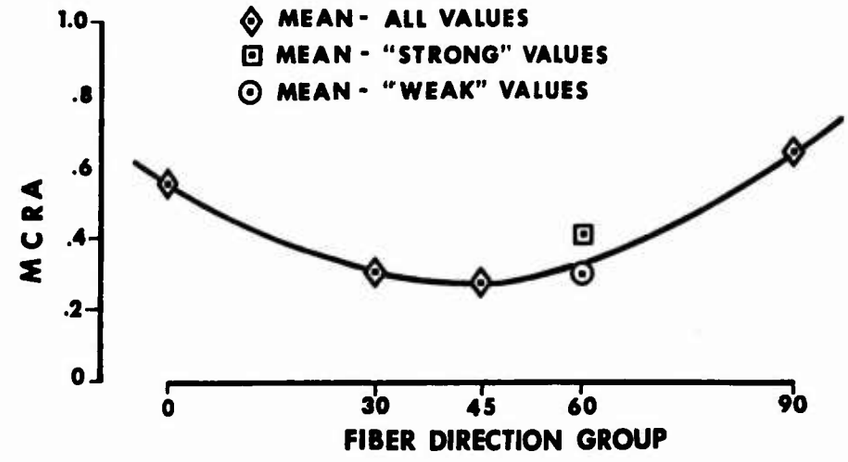

Figure 19. Mean Critical Rotation Angle (MCRA) Variation With Fiber Direction Group.

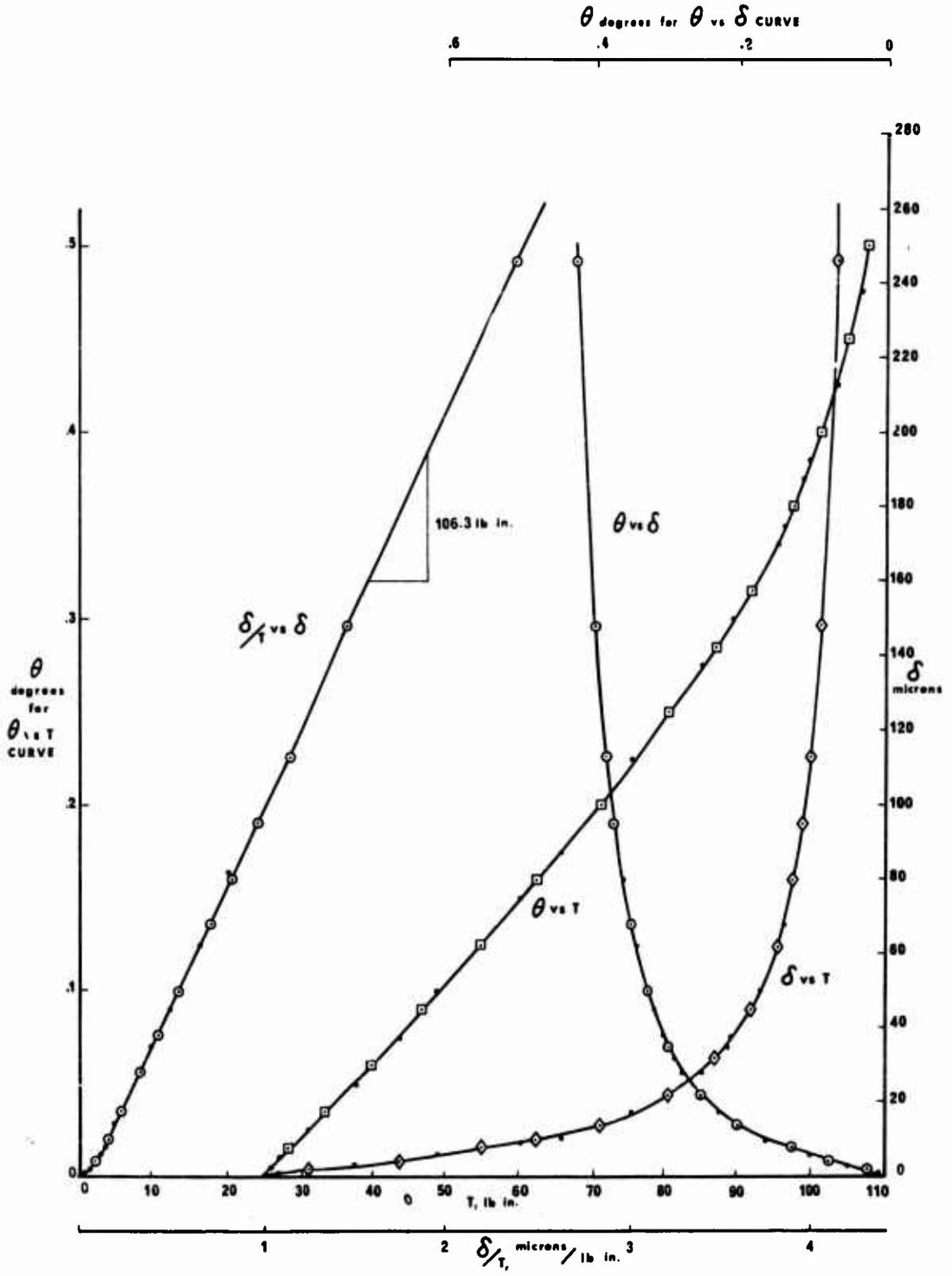

(a). Cylinder 002, 0°.

Figure 20. Southwell Plot and Other Data From Test of Cylinders.

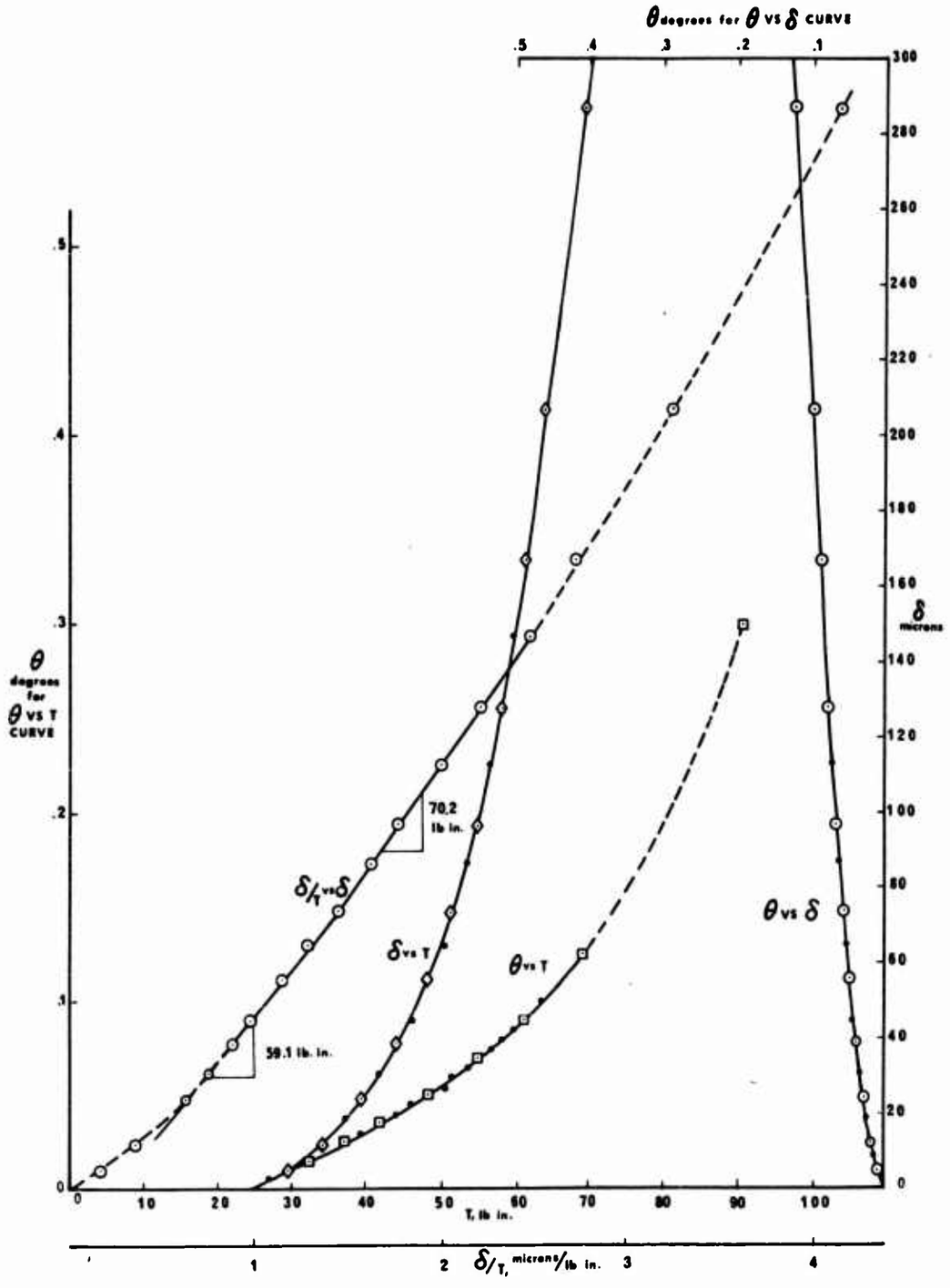

(b). Cylinder MU, 30°.

Figure 20. Continued.

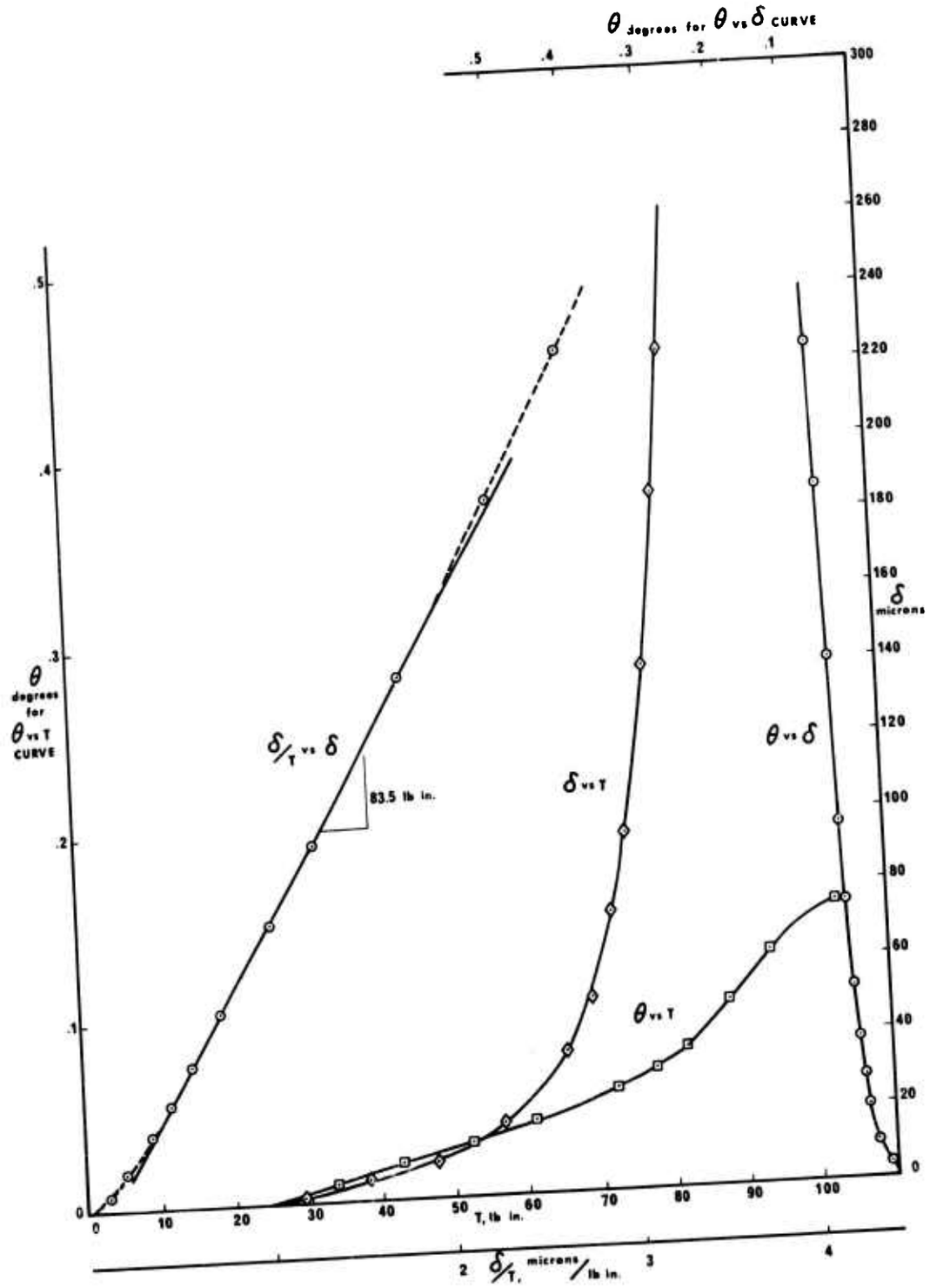

(c). Cylinder 065, 45°.

Figure 20. Continued.

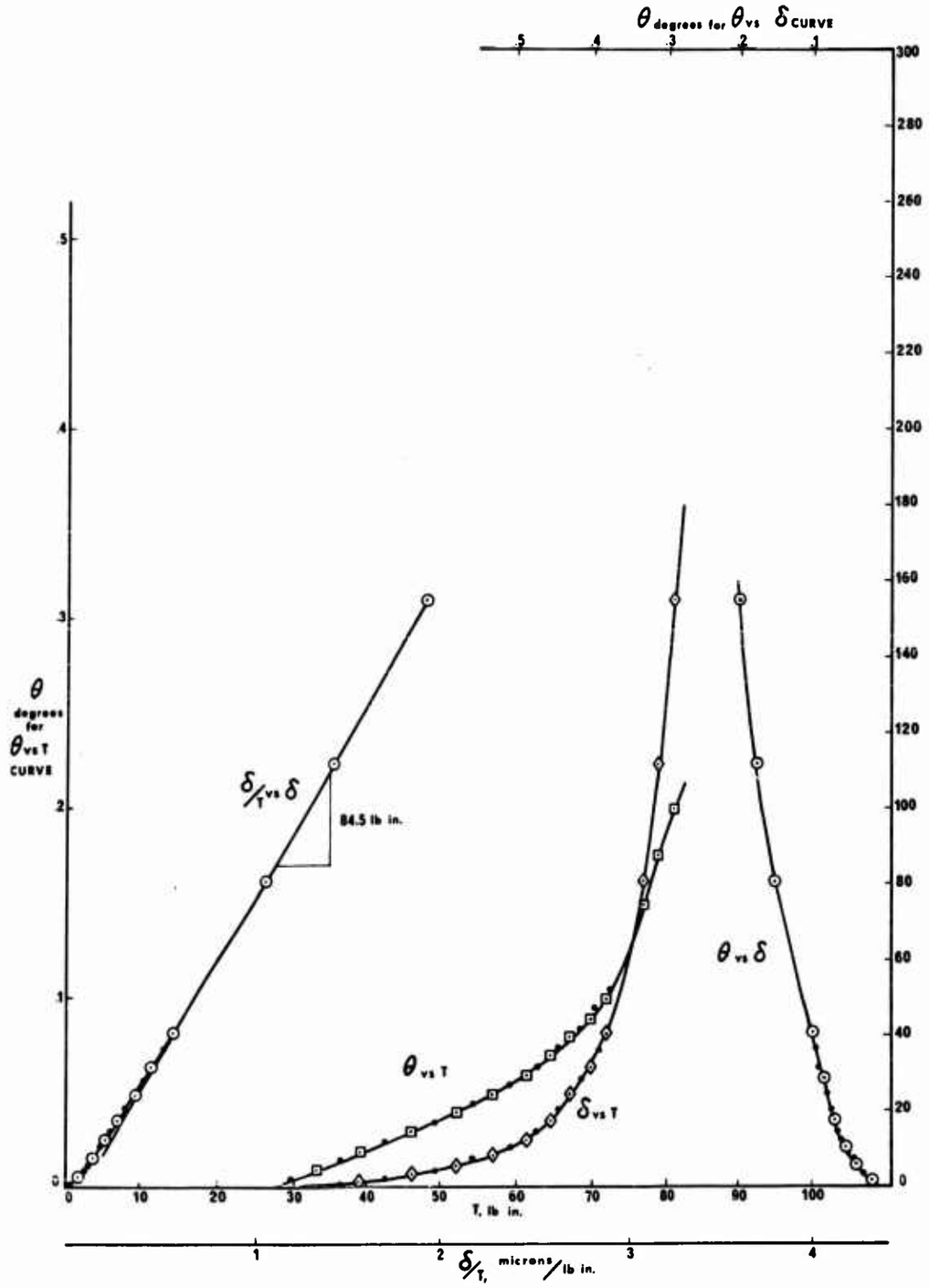

(d). Cylinder E, 53°.

Figure 20. Continued.

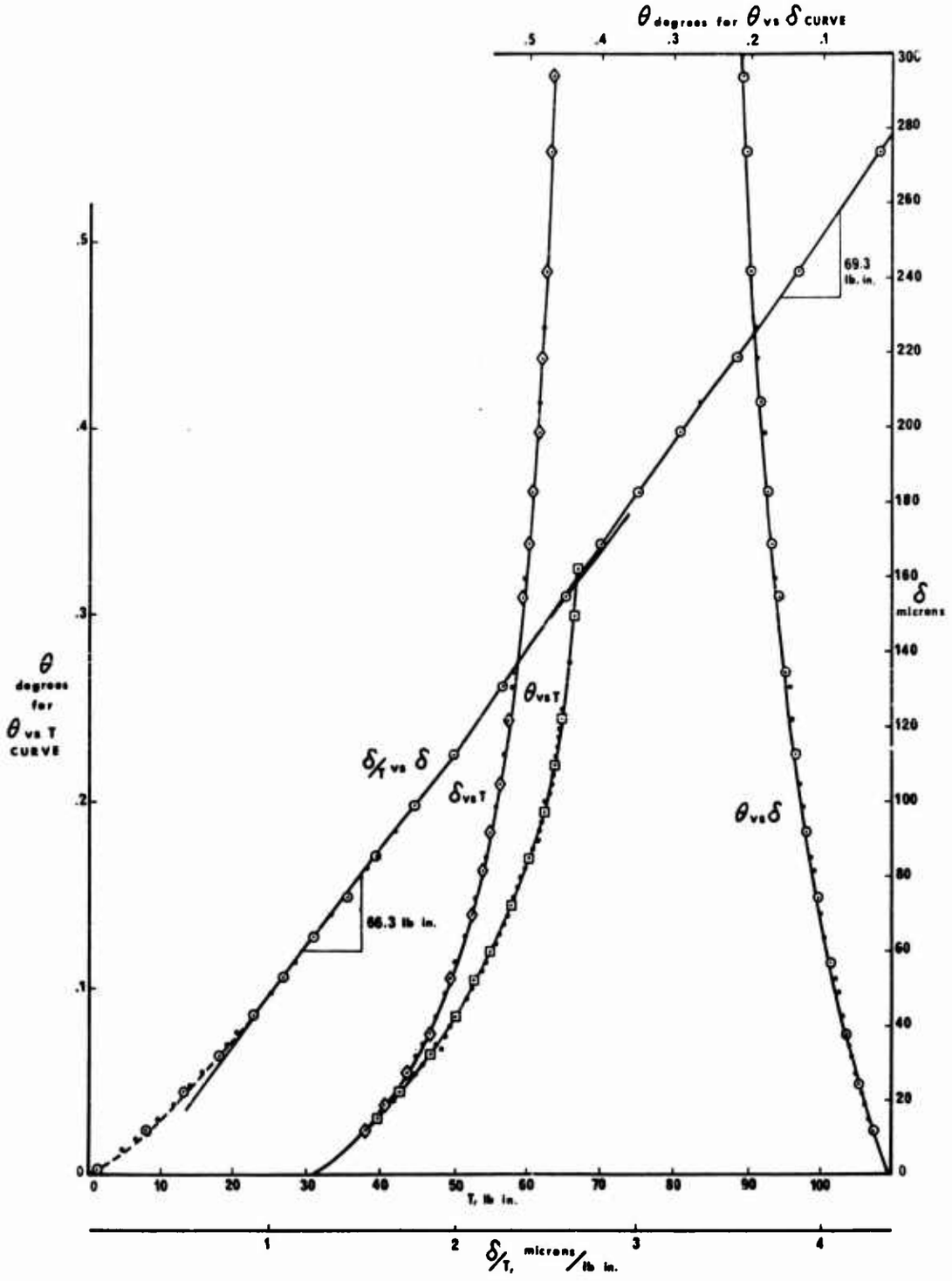

(e). Cylinder 069, 60°.

Figure 20. Continued.

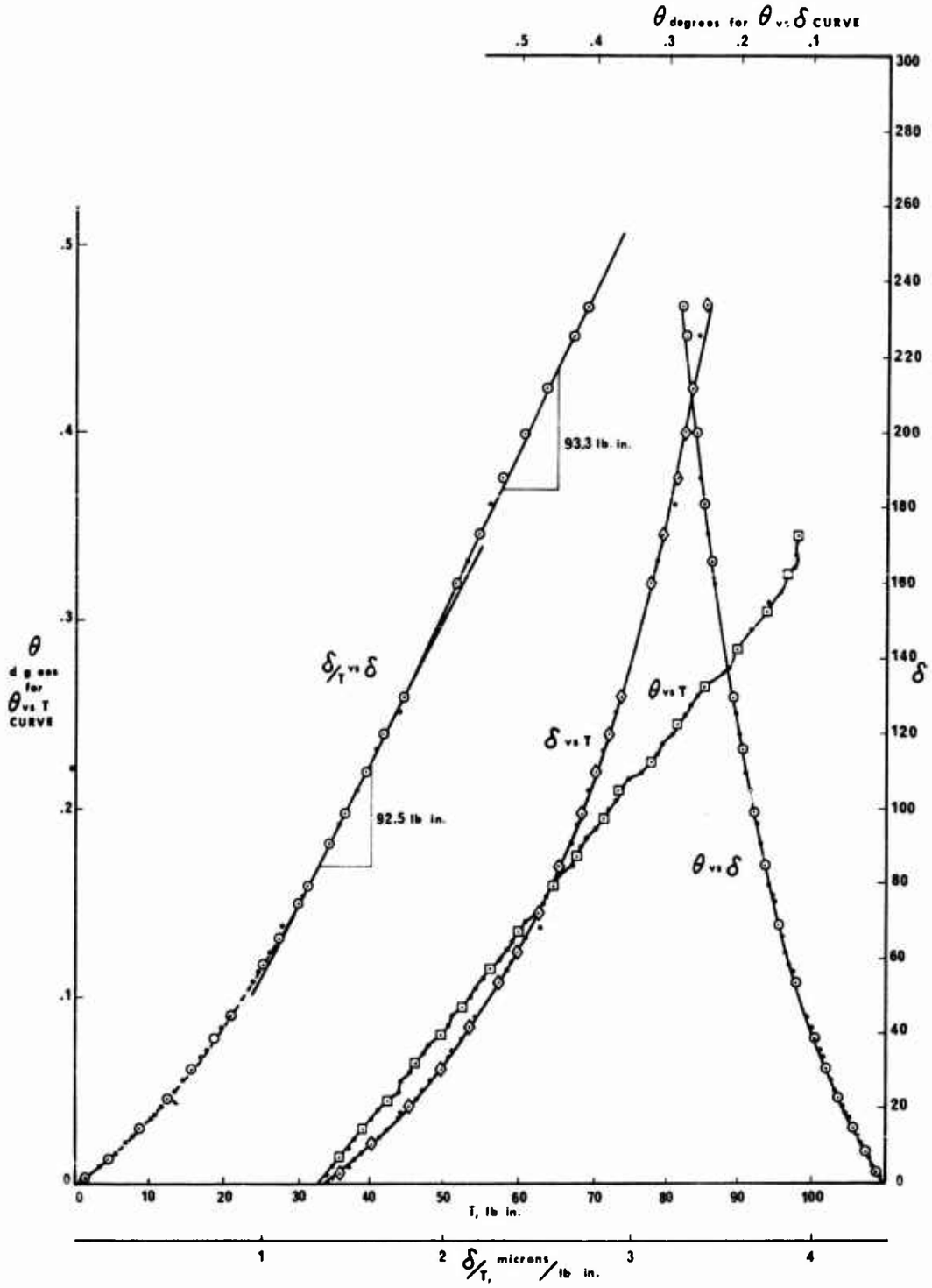

(f). Cylinder 072, 90°.

Figure 20. Continued

APPARENT DIRECTION DEPENDENCE WITHIN A FIBER DIRECTION GROUP

It was noticed during testing that with very few exceptions, the 0° and 90° specimens exhibited a "direction preference"; that is, the critical torque was higher in one direction than in the other. This direction preference generally was small but repeatable on a given specimen. The preferred direction in most cases was counterclockwise; but in 9 of 37 cases, it was clockwise. Alternation of initial test direction did not have any effect on the occurrence of the preference nor did alternation of seaming direction have any effect on the mandrel. Variation of fiber angles within a fiber angle group was too small to be responsible for the preference shown. It remains unexplained.

CONCLUSIONS

The experiments reported herein demonstrate that fiber direction is of importance in both torsional buckling strength and torsional stiffness of single-layer resin-impregnated glass-cloth cylinders. It was also shown that increasing torsional strength by choice of fiber orientation implies reducing torsional rigidity; trade-offs must be made.

REFERENCES

1. Nash, W. A, BIBLIOGRAPHY ON SHELLS AND SHELL-LIKE STRUCTURES, TMB Report 863, David Taylor Model Basin, U. S. Navy Department, Washington, D. C. (1954).

2. Nash, W. A., BIBLIOGRAPHY ON SHELLS AND SHELL-LIKE STRUCTURES, (1954-1956). University of Florida, Contract DA-01009-ORD-404, Office of Ordnance Research, U. S. Army (1957).

3. MIL-HDBK-17 PLASTICS FOR FLIGHT VEHICLES. Part I, Reinforced Plastics, Chapter 2, as revised 1 May 1964.

4. Minecci, J. J., THE EFFECT OF FIBER DIRECTION ON THE INSTABILITY OF SINGLE-LAYER GLASS-CLOTH RESIN-IMPREGNATED CYLINDERS UNDER UNIFORM AXIAL COMPRESSION, Engineer's Degree Thesis, Stanford University, March 1966.

5. Cheng, S., and Ho, B. P. C.,STABILITY OF HETEROGENEOUS AEOLOTROPIC CYLINDRICAL SHELLS UNDER COMBINED LOADING. AIAA Journal, Vol. 1, No. 4, pp. 892-898, April 1963.

6. Ho, B. P. C., and Cheng, S., SOME PROBLEMS IN STABILITY OF HETERO-GENEOUS AEOLOTROPIC CYLINDRICAL SHELLS UNDER COMBINED LOADING. AIAA Journal, Vol. 1, No. 7, pp. 1603-1607, July 1963.

7. Ambartsumian, S. A., CONTRIBUTIONS TO THE THEORY OF ANISOTROPIC LAYERED SHELLS. Applied Mechanics Review, Vol. 15, pp. 245-249, 1962.

8. Westergaard, H. M., BUCKLING OF ELASTIC STRUCTURES. Transactions of the American Society of Civil Engineers, Vol. 85, pp. 576-654, 1922.

9. Horton, W. H., and Bailey, S. C., THE SIGNIFICANCE OF TEST MACHINE RIGIDITY ON THE INITIAL BUCKLING LOAD FOR UNREINFORCED CIRCULAR CYLINDRICAL SHELLS IN AXIAL COMPRESSION. ASTM Paper 204, presented at the ASTM Annual Meeting in Atlantic City, N. J., June 1966.

10. Sturm, R. G., A STUDY OF THE COLLAPSING PRESSURE OF THIN-WALLED CYLINDERS. University of Illinois Engineering Experiment Station Bulletin, Series No. 320, Vol. XXXIX, Nov. 11, 1941, No. 12.

11. Horton, W. H., and Durham, S. C., THE EFFECT OF RESTRICTING BUCKLE DEPTH IN CIRCULAR CYLINDRICAL SHELLS REPEATEDLY COMPRESSED TO THE BUCKLING LIMIT. SUDAER 174, November 1963.

12. Horton, W. H., and Cox, J. W., THE STABILITY OF THIN-WALLED UNSTIFFENED CIRCULAR CYLINDRICAL SHELLS UNDER NONUNIFORMLY DISTRIBUTED AXIAL LOAD. SUDAER 220, February 1965.

13. Southwell, R. V., ON THE ANALYSIS OF EXPERIMENTAL OBSERVATIONS IN PROBLEMS OF ELASTIC STABILITY, Proceedings of the Royal Society, A, Vol. 135, pp. 601-616, 1932.

14. Gough, H. J., and H. L. Cox, SOME TESTS ON THE STABILITY OF THIN STRIP MATERIAL UNDER SHEARING FORCES, Proceedings of the Royal Society, A, Vol. 137, pp. 145-157, 1932.

15. Southwell, R. V., and Skan, S. W., ON THE STABILITY UNDER SHEARING FORCES OF A FLAT ELASTIC STRIP, Proceedings of the Royal Society, A., Vol. 105, p. 582, 1924.

16. Gregory, M., THE APPLICATION OF THE SOUTHWELL PLOT ON STRAINS TO DETERMINE THE FAILURE LOAD OF A LATTICE GIRDER WHEN LATERAL BUCKLING OCCURS, Austrailian Journal of Applied Mechanics, Vol. 10, pp. 371-376, 1959.

17. Gregory, M., THE APPLICATION OF THE SOUTHWELL PLOT ON STRAINS TO PROBLEMS OF ELASTIC INSTABILITY OF FRAMED STRUCTURES WHERE BUCKLING OF MEMBERS IN TORSION AND FLEXURE OCCURS, Austrailian Journal of Applied Mechanics, Vol. 11, pp. 49-64, 1960.

18. Horton, W. H., Cundari, F., and Johnson, R., THE ANALYSIS OF EXPERIMENTAL DATA OBTAINED FROM STABILITY STRUCTURES ON ELASTIC COLUMNS AND PLATE STRUCTURES, Report in preparation at Stanford University.

APPENDIX
SOUTHWELL PLOT

In 1922, Westergaard[8] developed a generalized theory of elastic stability which suggests that under certain conditions the relationship between displacement and the force which produces it can be expressed to a first approximation in a hyperbolic form. This suggestion was not entirely new; it had, in fact, been proposed by earlier researchers for the strut. Little use, however, had been made of this property until it was rediscovered by Southwell[13] in 1932 and applied by him to the interpretation of data obtained in tests on struts. Subsequently, Gough and Cox [14] verified the theoretical treatment of the problem of shear buckling in a flat, elastic strip by Southwell and Skan[15], using the Southwell plot to determine the theoretical critical load for the strips. More recently, Gregory has shown that the Southwell plot is applicable to lateral buckling of lattice girders[16] and buckling of framed structures in torsion and flexure[17]. Horton, Cundari, and Johnson[18] have analyzed data on the stability of columns and plates using the Southwell Plot, and a similar study for shell bodies is currently being prepared.

As an adjunct to the primary line of investigation, several tests were made to determine the feasibility of applying the Southwell plot to the torsional stability of heterogeneous, aeolotropic, cylindrical shells such as those used in this investigation. For these tests, measurements were made of the radial deflection of a "quasi-random" point on the specimen in addition to the standard measurements made on all tests.

The points at which measurements of radial deflection were taken were not truly random, since they were required to be on the centerline of a buckle flute as determined from a previous test. This requirement was dictated by the fact that although the Fotonic Sensor is primarily sensitive to linear displacement, it is also affected by rotations of the viewed area. Rotations are clearly minimized at the centerline of a flute.

The results of tests on a specimen from each of the five fiber direction groups and one special specimen are presented in Table IV and Figure 20. All six tests produced usable straight lines on the Southwell plot. Of these, four had slopes within 5 percent from the critical value, and one was 20.9 percent off. Five of the six tests produced Southwell slopes predicting instability at load levels lower than those actually carried, while the sixth predicts a load level slightly higher than that carried. Three of the curves, when plotted on a large scale, show two distinct straight-line segments of slightly different slope.

The fact that Southwell plots of the data from these tests give extremely good, straight lines can only be interpreted as being consistent with the hyperbolic nature of the load-displacement relationship. The question of whether the slope of this line corresponds to the critical load for a perfect shell could not be resolved, since an adequate theoretical description of the problem is not currently available. Further research on the question appears to be warranted.